Journal of Manufacturing Processes 101 (2023) 737–754

Contents lists available at ScienceDirect

Journal of Manufacturing Processes

journal homepage: www.elsevier.com/locate/manpro

# Investigation of variability in apparent values of materials properties in thermo-mechanical uniaxial tensile tests on sheet metals

Ruiqiang Zhang, Jun Jiang *, Jianguo Lin, Victoria A. Yardley

*Department of Mechanical Engineering, Imperial College London, London SW7 2AZ, UK*

ARTICLE INFO

*Keywords:*
Thermo-mechanical tests
Temperature
Strain rate
Hot stamping
Gauge length
Stress–strain curves

ABSTRACT

Thermo-mechanical uniaxial tensile testing is commonly carried out to characterise the mechanical properties of materials under conditions which mimic advanced industrial forming processes, such as hot stamping of steels and aluminium alloys, and to generate microstructures for metallographic investigation. However, in this type of testing, heat loss to the specimen grips can lead to nonuniform temperature distributions along the gauge length, resulting in challenges in determining absolute values of materials properties at the nominal temperature of interest. The present study investigates the effect of these nonuniform temperature distributions on the variability in the thermo-mechanical properties as measured in the tests, and in the microstructures of the tested specimens. For this purpose, uniaxial tensile tests on the boron steel 22MnB5 and aluminium alloy AA6082 were performed under hot stamping conditions using a Gleeble 3800 thermal-mechanical physical simulation system, in which the specimens were heated using resistance heating and the strain fields were measured using digital image correlation (DIC). The nonuniformity of the temperature distributions along the gauge length was quantified. Both the strains and the strain rates along the gauge length were then computed and the effects of factors such as pre-forming gauge length, post-forming gauge length and specimen design on the spatial distribution of strains and strain rates were investigated. The effects of these factors on the values of thermo-mechanical properties determined from the tests, such as the ductility and the ultimate tensile strength (UTS), were also analysed and quantified. This study reveals the variability in the apparent values of materials properties as determined by thermo-mechanical testing resulting from nonuniform temperature distributions, and provides experimental data for the development of new standards for thermo-mechanical tests in future.

## 1. Introduction

Steel and aluminium alloy sheet materials are the main materials currently applied in the manufacture of lightweight body structures in the automotive industry because of their high tensile strength and high stiffness-to-weight ratios [1]. However, these materials exhibit only moderate formability at room temperature, limiting their industrial applications [2]. In contrast, warm or hot forming of these sheet metals, in which the sheet material is deformed to the target shape at high temperatures, can significantly improve their formability [3,4]. For example, the percentage elongation at fracture, a measure of ductility, of the boron steel 22MnB5 can reach ~60% at hot stamping temperatures, which is 200% higher than that (i.e. ~20%) at room temperature. Standard methods exist for the tensile testing of metallic materials at both room temperature and elevated temperatures [5,6]; these are routinely used for the determination of mechanical properties such as yield strength, ultimate tensile strength (UTS), and elongation. One important application of such testing is for the investigation of warm or hot forming technologies, for which it is essential to precisely characterise the thermo-mechanical properties and microstructural features of the materials under conditions which mimic those warm or hot forming processes.

Thermo-mechanical tensile tests have been carried out extensively for the characterisation of high-temperature deformation behaviour of sheet metals (for example in [7,8]). In these tests, sheet material is heated to its target temperature using either direct heating methods such as induction heating [9,10] as shown in Fig. 1(a), or indirect heating methods such as furnaces [11,12] as shown in Fig. 1(b). More recently, the Gleeble thermo-mechanical simulator has been used for testing of sheet metal at hot stamping temperatures [13–15]; here, the test specimen is heated using the direct resistance heating method and a pair of thermocouples is used to provide signals for accurate feedback control of

* Corresponding author.
*E-mail address:* jun.jiang@imperial.ac.uk (J. Jiang).

https://doi.org/10.1016/j.jmapro.2023.06.005
Received 15 March 2023; Received in revised form 30 May 2023; Accepted 6 June 2023
Available online 24 June 2023

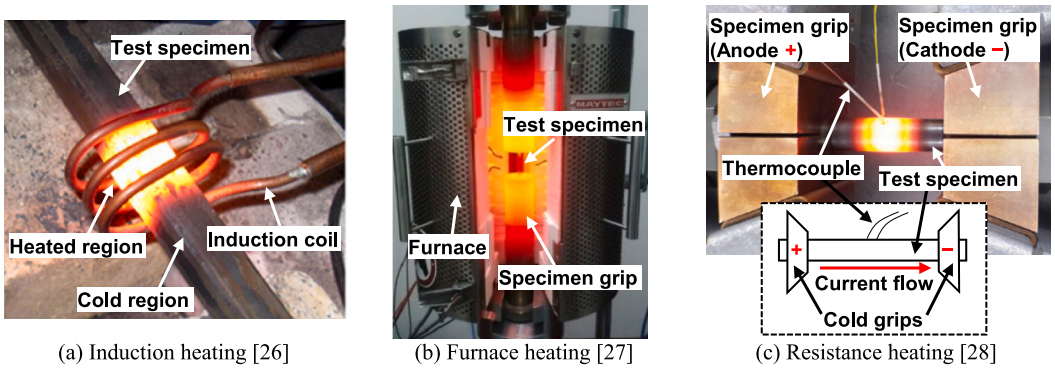


(a) Induction heating [26] (b) Furnace heating [27] (c) Resistance heating [28]

**Fig. 1.** Existing heating methods to heat samples for thermo-mechanical tests [26-28].

the temperature at a given location, usually the specimen centre (Fig. 1 (c)). In real hot stamping operations, the material must be quenched quickly before deformation occurs [16]; the Gleeble system has a cooling system and the capability to precisely control both the heating and cooling rate over a wide range. For example, it is able to rapidly quench samples to an intermediate temperature to enable deformation to be performed at this temperature [17]. However, it has been found that in uniaxial tensile tests in the Gleeble system, temperature distributions along the gauge length are nonuniform [18–21]; the temperature is highest at the specimen centre and decreases with increasing distance from it. This temperature heterogeneity is due to heat loss to the specimen grips, which are water-cooled for safety reasons (inset in Fig. 1(c)). Much research effort has been dedicated to avoiding or minimising such temperature heterogeneities [22]. However, there is currently no method that is capable of fully eliminating them, and it is very likely that some degree of nonuniformity in temperature is inevitable in thermo-mechanical tests using the Gleeble system. It should be noted that such nonuniformities are not restricted to the Gleeble system, but also occur in other thermo-mechanical testing systems in which there is heat transfer from the gauge area to other parts of the system [23–25].

Several studies have investigated the effects of the nonuniform temperature distributions on the results of thermo-mechanical tests carried out using the Gleeble system [29–31]. Kardoulaki et al. [29] found, using numerical assessment, that strain distributions in the gauge length of cylindrical specimens of steel deformed with thermal gradients were significantly less uniform than those deformed isothermally. Shao et al. [30] quantified the nonuniformity of the temperature distributions along dog-bone specimens of aluminium alloy AA6082 sheets under hot stamping conditions, and numerically analysed both the stress and strain distributions along the gauge length and the errors in the true stress–true strain curves caused by the nonuniform temperature distributions. Zhang et al. [31] were the first researchers to successfully measure the full strain fields of boron steel sheet specimens at hot stamping temperatures (up to 950 °C) using digital image correlation (DIC). Using the strain fields measured, this study determined both the strain and strain rate distributions along the gauge length throughout deformation. For the interpretation of the results, several different virtual or effective gauge lengths were used for evaluating the ductility of the material; virtual gage length is a shorter length over which the temperature can be considered to be reasonably uniform. It was found that both the average strain and the average strain rate depended increasingly on the choice of virtual gauge length with increasing time since the beginning of the deformation, and the ductility as evaluated depended on the virtual gauge length that was chosen.

The above publications demonstrate that thermal gradients exist along the gauge length, and that these gradients cause spatial heterogeneities in strain and strain rate. However, no studies have so far been carried out to investigate the influence of the method of controlling the strain rate and of the specimen design on the distributions of temperature, strain and strain rate, and on the thermo-mechanical properties measured. In addition, there is currently a lack of standards for thermo-mechanical tensile tests in which the temperature distribution along the gauge length is nonuniform.

The aim of the present study is to investigate the variability in the

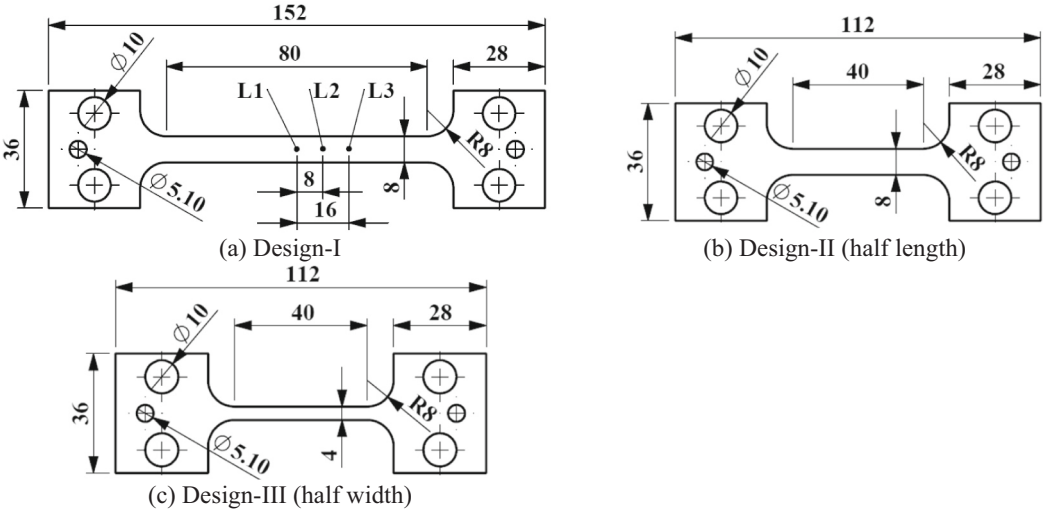


(a) Design-I (b) Design-II (half length)

(c) Design-III (half width)

**Fig. 2.** Geometries and dimensions of the three dog-bone specimen designs used in the present study for thermo-mechanical tests on boron steel and aluminium alloy sheets. L1, L2 and L3 are locations on specimens for analysing deformation along the gauge length.

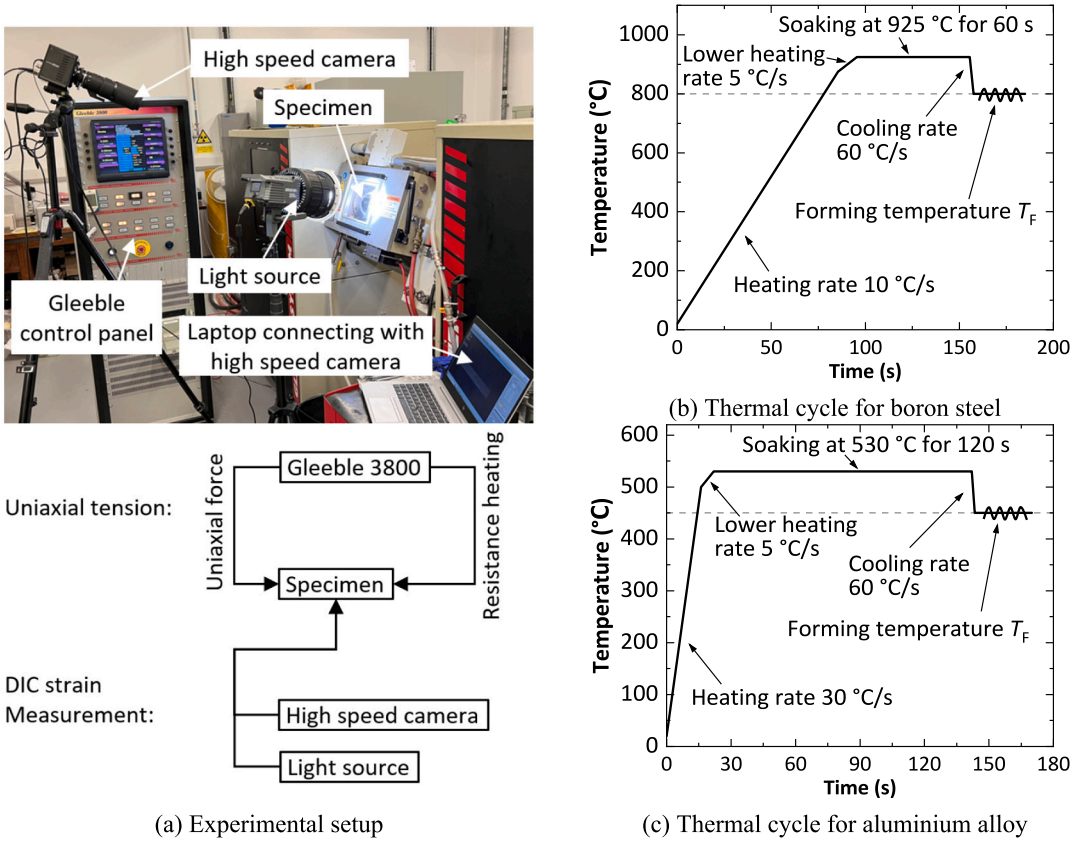


**Fig. 3.** Experimental setup and thermal cycles for thermo-mechanical tests on boron steel and aluminium alloy sheets to mimic industrial hot stamping conditions for these materials.

apparent values of materials properties obtained in thermo-mechanical tests as a result of nonuniformities in temperature distribution along the gauge length. Uniaxial tensile tests on sheet metal specimens under hot stamping conditions have been performed using the Gleeble system, and distributions of temperature, strain and strain rate along the gauge length have been quantified. In addition, engineering stress–engineering strain curves, giving values of ductility and UTS have been determined using the average strain value obtained over a chosen a post-forming gauge length. The test method and evaluation of mechanical properties require the choice of values for a pre-forming gauge length and a post-forming gauge length. The effects of the pre-forming gauge length, post-forming gauge length and the specimen design on the engineering stress–engineering strain behaviour and apparent values of the mechanical properties were investigated and quantified.

## 2. Methodology

### 2.1. Materials and specimen designs

The materials used in the present study are zinc-coated boron steel 22MnB5 sheets and aluminium alloy AA6082 sheets, both of thickness 1.5 mm. The chemical composition of 22MnB5 is Fe-0.20C-1.17Mn-0.25Si-0.20Cr-0.002S-0.0029B-0.028Ti-0.001Nb-0.023Ni (wt%), and the composition of AA6082 is Al-0.87Si-0.33Fe-0.026Cu-0.51Mn-0.97Mg-0.044Cr-0.025Zn-0.016Ti (wt%). To investigate the effect of specimen dimensions on apparent values of materials properties obtained in thermo-mechanical tests, three dog-bone specimen designs, Design-I, Design-II and Design-III, are adopted; these are shown in Figs. 2(a), 2(b) and 2(c), respectively. The only differences among the designs are the length $L_0$ and width $W_0$ of the gauge area. Design-I has $L_0$ = 80 mm, and $W_0$ = 8 mm, while in Design-II, $L_0$ is reduced by half, namely $L_0$ = 40 mm and in Design-III, both $L_0$ and $W_0$ are reduced by half, namely $L_0$ = 40 mm, and $W_0$ = 4 mm. All specimens were cut with the long direction of the gauge area parallel to the rolling direction of the as-received sheets.

### 2.2. Experimental setup and testing conditions

All the thermo-mechanical tests in the present study were carried out using a Gleeble 3800 thermo-mechanical simulator system. Fig. 3(a) shows a photograph and schematic flowchart of the experimental setup. During the tests, the Gleeble provided electric current to heat the specimens using the direct resistance heating method, high pressure air to cool the specimens, and uniaxial forces to stretch them. A pair of K-type thermocouples was welded at the specimen centre to monitor the temperature at this location using the Gleeble, and then provided signals to the Gleeble for accurate feedback control the specimen temperature during heating and quenching processes. Full-field strains were measured using a digital image correlation (DIC) system which includes a high-speed camera (Photron FASTCAM Mini UX50) and a light source (Amaran 200d LED). To mimic industrial hot stamping conditions, the thermal cycles shown in Figs. 3(b) and 3(c) were applied to the boron steel and aluminium alloy, respectively. In Fig. 3(b), the boron steel material is heated up to 925 °C and soaked at the temperature for 60 s to give full austenitisation [32]. The material is then quenched at a rate of 60 °C/s to a forming temperature $T_F$, then deformed for the characterisation of thermomechanical behaviour. In Fig. 3(c), the aluminium alloy material is heated to 530 °C and soaked at this temperature for 120 s, representing the solution heat treatment (SHT) stage of hot stamping, then quenched at 60 °C/s to the target temperature $T_F$ for the thermo-mechanical testing [33]. To measure the temperature distributions along the gauge length, the temperatures at several different locations on the specimens were measured using the Gleeble and K-type thermocouples. Since the specimen designs and their thermal boundary

**Table 1**
Testing conditions for the thermo-mechanical tests on boron steel and aluminium alloy sheets.

| Material | Specimen design | Temperature (°C) | Strain rate (/s) | Pre-forming gauge length $l_{Pre}$ (mm) |
|---|---|---|---|---|
| Boron steel 22MnB5 | Design-I | 750 | 0.1 | $2\times W_0$=16 |
| | | 750 | 0.5 | $W_0$ is initial |
| | | 850 | 0.1 | specimen width |
| | | 850 | 0.5 | |
| | | 750 | 0.1 | 32 |
| | | 750 | 0.5 | |
| | | 850 | 0.1 | |
| | | 850 | 0.5 | |
| | Design-II & Design-III | 750 | 0.1 | 16 |
| | | 750 | 0.5 | |
| | | 850 | 0.1 | |
| | | 850 | 0.5 | |
| Aluminium alloy AA6082 | Design-I | 375 | 0.1 | 16 |
| | | 450 | 0.5 | |

conditions were symmetrical, it was assumed that the temperature distributions were also symmetrical about the specimen centre [22]. Only the temperatures in one half of the gauge area were therefore measured.

To obtain the target strain rates during the thermo-mechanical tests, Eq. (1) below was used to calculate the displacement of the specimen grips $\Delta l$ that is required to stretch the specimens, where $l_{Pre}$ ($l_{Pre} \le L_0$) is the pre-forming gauge length, which is a virtual value used in Eq. (1) for this purpose. It should be noted that Eq. (1) was derived under the assumption of uniform deformation within the gauge length.

$$\Delta l = l_{Pre} \bullet \left[ exp\left( \Delta t \bullet \dot{\varepsilon}_T \right) - 1 \right] \quad (1)$$

Here, $\Delta l$ is the total change in displacement from the beginning of deformation to a total time $\Delta t$, $l_0$ is the initial gauge length, and $\dot{\varepsilon}_T$ is the target strain rate.

Table 1 lists all the thermo-mechanical testing conditions used in the present study. For the boron steel, the tests were carried out at a temperature of 750 and 850 °C and at a strain rate of 0.1 and 0.5 /s to investigate the effect of temperature and strain rate on the variability in thermo-mechanical test results. A pre-forming gauge length $l_{Pre}$ of 16 mm was selected according to experience. An alternative value of $l_{Pre}$ = 32 mm was also used to study the variability in apparent mechanical properties caused by changing this parameter. In addition, the three different specimen designs shown in Fig. 2 were used to investigate their influence on the results of thermo-mechanical tests. The tests on the aluminium alloy were carried out to quantify the variability in apparent values of mechanical properties for a different material.

### 2.3. Speckle patterns and data processing for strain measurement using DIC

To use the DIC for strain measurement, random speckle patterns were prepared beforehand on the specimen surfaces that were to face the high-speed camera during the tests [31]. These patterns consist of a thin black background with many fine white dots painted using an air brush, and will be shown in Section 3.1.2. The VHT FLAMEPROOF™ black coating SP102 and white coating SP101 which can withstand temperatures up to 1093 °C were used for the patterns in the present study. Before painting, all samples were ground to remove coatings if applicable (e.g. zinc coating on 22MnB5) and oxidisation layers, and then cleaned using acetone. The frame rate of the high-speed camera for recording the deformation was related to the strain rate (i.e. total deformation time); according to experience, 250 frames per second (fps) was chosen for the tests at 0.1 /s, and 500 fps for 0.5 /s. All the deformation images recorded were post-processed using the commercial software GOM Correlate, setting the software parameters of facet size to 19 pixels and point distance to 10 pixels. The strain fields in the specimen gauge area excluding the area near the edges of the gauge area (less than 1 mm along the width direction) were determined, which will be shown in Section 3.1.2.

### 2.4. Microstructural characterisation

To reveal the microstructure and phase distribution in the boron steel 22MnB5, the material was ground using abrasive papers with grit size from P800 to P4000, and then polished using 1 μm polycrystalline diamond suspension. Finally, the polished surface was etched using 2% Nital for about 5 s [34]. Micrographs were obtained using a scanning electron microscope (SEM) (TESCAN, Czechia), operated with a voltage of 15 kV and a beam current of 1 nA.

## 3. Results

### 3.1. Distributions of temperature and strain along the gauge length

#### 3.1.1. Temperature distributions

The temperature distributions along the length direction of the specimens are shown in Fig. 4(a) for the boron steel and Fig. 4(b) for the

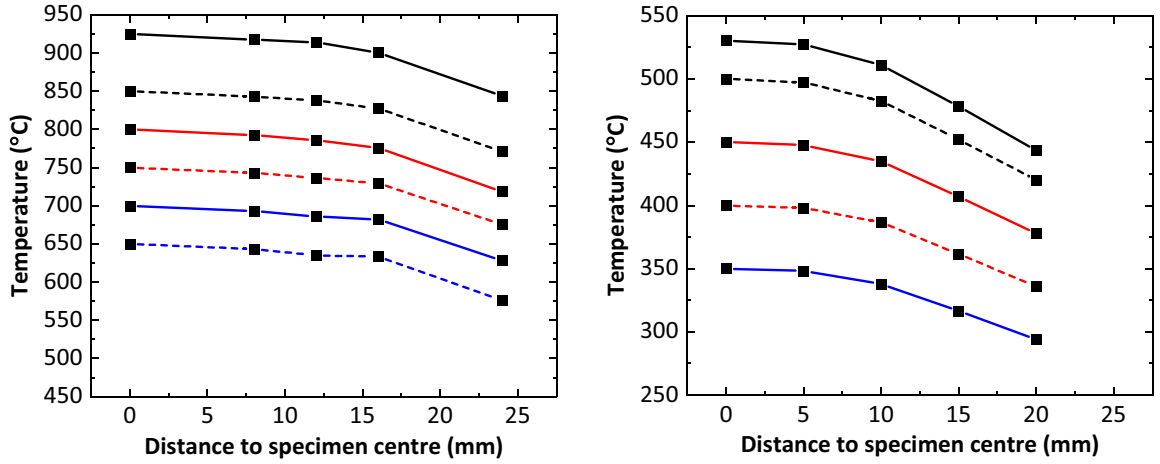


(a) Boron steel 22MnB5 (b) Aluminium alloy AA6082

**Fig. 4.** Temperature distributions along the length direction of the specimens with Design-I when the temperature at the specimen centre had stabilised at the target value. The different lines represent the temperature distributions when the specimen centre was heated to different temperatures, such as 650 °C, 700 °C, 750 °C, etc.

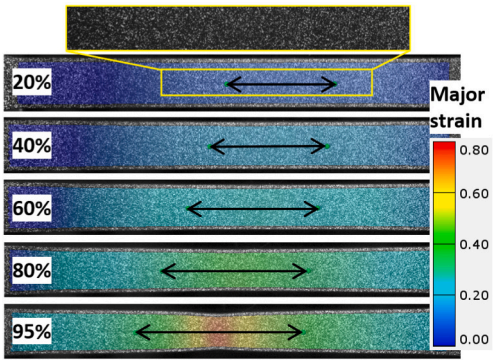


(a) Strain fields at 750 °C & 0.1 /s

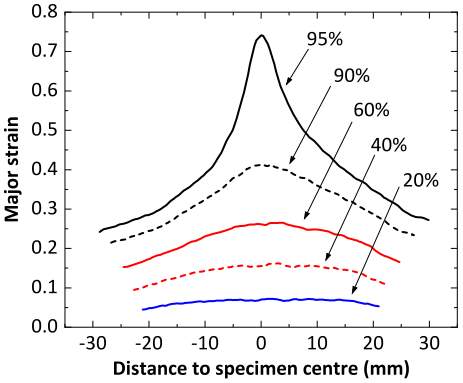


(b) Strain distributions at 750 °C & 0.1 /s

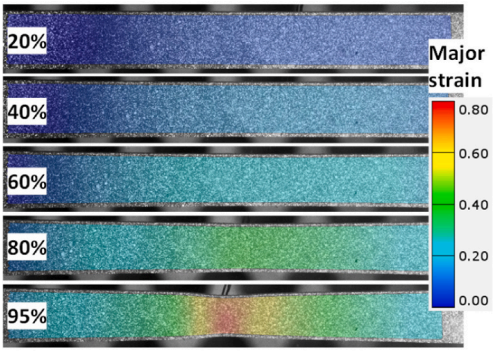


(c) Strain fields at 750 °C & 0.5 /s

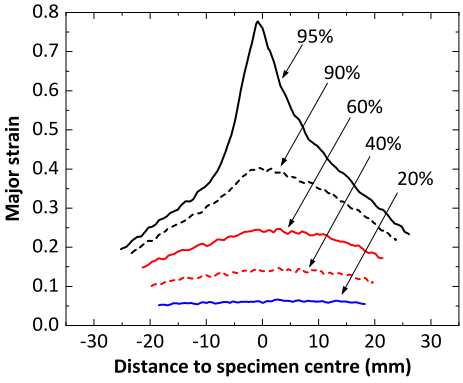


(d) Strain distributions at 750 °C & 0.5 /s

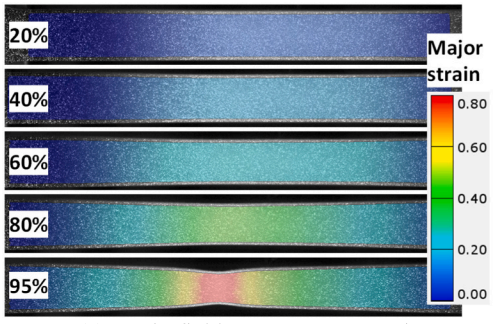


(e) Strain fields at 850 °C & 0.1 /s

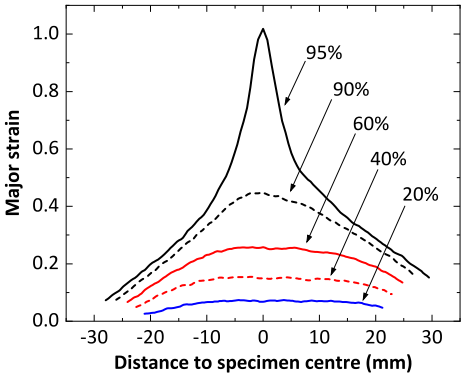


(f) Strain distributions at 850 °C & 0.1 /s

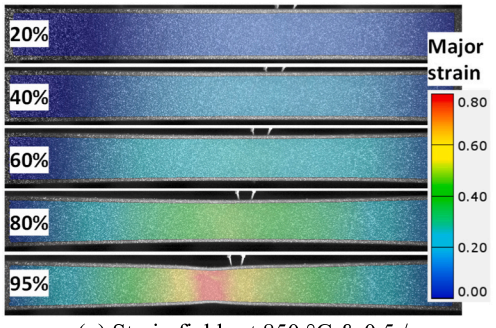


(g) Strain fields at 850 °C & 0.5 /s

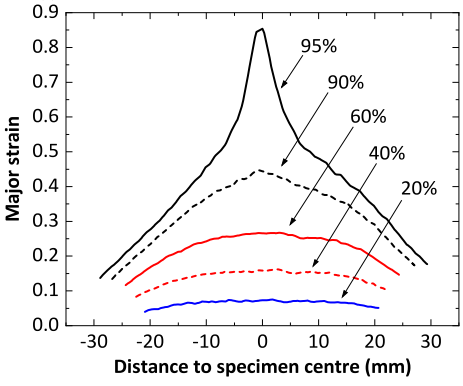


(h) Strain distributions at 850 °C & 0.5 /s

**Fig. 5.** Major strain (or axial strain) fields and their distributions along the long axis of the boron steel 22MnB5 specimens (Design-I) under different test conditions. All tests were performed using a pre-forming gauge length $l_{Pre}$ of 16 mm. The values 20%, 40%, 60%, 80% and 95% are normalised times $t/t_F$. In (a), inset shows the speckle patterns, and black arrow shows a post-forming gauge length $l_{Post}$ of 16 mm for data post-processing in the following sections.

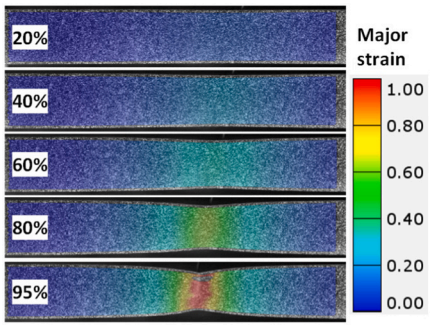


(a) Strain fields at 375 °C & 0.1 /s

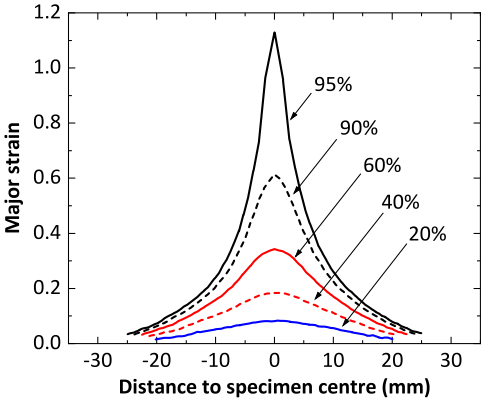


(b) Strain distributions at 375 °C & 0.1 /s

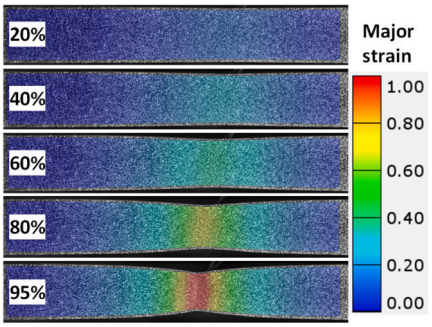


(c) Strain fields at 450 °C & 0.5 /s

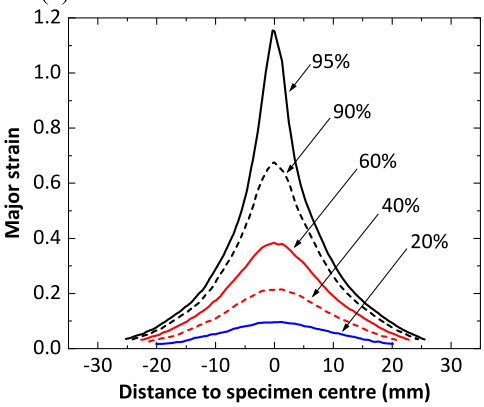


(d) Strain distributions at 450 °C & 0.5 /s

**Fig. 6.** Major strain (or axial strain) fields and their distributions along the long axis of the aluminium alloy AA6082 specimens (Design-I) under different test conditions. All tests were carried out using a pre-forming gauge length $l_{Pre}$ of 16 mm. The values 20%, 40%, 60%, 80% and 95% are normalised times $t/t_F$.

aluminium alloy. The data points on each curve were obtained when the temperature at the specimen centre had stabilised at the target value. It can be seen that, in both materials, the specimen centre always had the highest temperature. With increasing distance ($D$) from the centre, the temperature decreased with an increasing gradient; this was more pronounced in the aluminium alloy specimens probably due to the fact that the thermal conductivity of aluminium alloy is higher than that of steel [35]. For example, in the boron steel specimens (Fig. 4(a)), when the temperature ($T_C$) at the specimen centre was 850 °C, it decreased by 0.008 (normalised by 850 °C) at $D = 8$ mm, 0.014 at $D = 12$ mm, 0.026 at $D = 16$ mm and 0.093 at $D = 24$ mm. In the aluminium alloy specimens (Fig. 4(b)), when $T_C = 450$ °C, it decreased by 0.005 (normalised by 450 °C) at $D = 5$ mm, 0.034 at $D = 10$ mm, 0.096 at $D = 15$ mm and 0.161 at $D = 20$ mm. The reason for the temperature decrease is heat loss to the specimen gauge regions and the water-cooled specimen grips [22].

### 3.1.2. Distribution and evolution of strain fields in the gauge area

Fig. 5 presents the full-field strains in the gauge area of the boron steel specimens, as measured using DIC, at different times $t$ normalised by the time $t_F$ at fracture ($t/t_F$ = 20%, 40%, 60%, 80% and 95%). The time $t_F$ of the tests conducted at different temperatures and strain rates is 8.840 s (at 750 °C & 0.1 /s), 1.654 s (at 750 °C & 0.5 /s), 7.950 s (at 850 °C & 0.1 /s) and 1.720 s (at 850 °C & 0.5 /s). As shown in Fig. 5(a), at 750 °C & 0.1 /s, the deformation became increasingly localised near the specimen centre, where the temperature was highest, with increasing normalised time. Fig. 5(b) shows the corresponding distributions of major strain (which, in uniaxial testing, is the strain along the long axis) along the gauge length; the localisation of the major strain near the specimen centre can be seen even in the early stages (e.g. $t/t_F$ = 20%) of deformation. Similar phenomena of strain localisation can also be observed in the tests carried out under the other conditions, i.e. at 750 °C & 0.1 /s (Figs. 5(c) and 5(d)), at 850 °C & 0.1 /s (Figs. 5(e) and 5(f)) and at 850 °C & 0.5 /s (Figs. 5(g) and 5(h)). Considering that it took place in the early stages, it can be concluded that the strain localisation must be caused by the nonuniform temperature distributions rather than, for example, by necking, which usually only occurs in the late stages of deformation.

Fig. 6 shows the strain fields in the gauge area of the AA6082 specimens, and their distributions along the gauge length, measured using the DIC, at different normalised times. As can be seen in Figs. 6(a)-(b), for the test at 375 °C & 0.1 /s and Figs. 6(c)-(d), for the test at 450 °C & 0.5 /s, the deformation became increasingly localised near the specimen centre with increasing time. This localisation can be seen even in the early stages (e.g. $t/t_F$ = 20%); these observations are similar to those in the 22MnB5 tests. However, the degree of deformation in the vicinity of the specimen centre is much higher in the AA6082 specimens throughout deformation than is the case in the 22MnB5 specimens. This was probably caused by the higher temperature gradients in the AA6082 specimens than in the 22MnB5 specimens, which can be seen in Fig. 4.

## 3.2. Effects of pre-forming gauge length $l_{Pre}$

### 3.2.1. Strains and strain rates

The effect of varying the value of the pre-forming gauge length $l_{Pre}$ in Eq. (1) was investigated using the values $l_{Pre}$ = 16 and 32 mm and the test conditions for 22MnB5 given in Table 1, using Design-I. As discussed in Section 2.2 above, $l_{Pre}$ ($l_{Pre} \leq L_0$) is a virtual value used to compute the required displacement of the specimen grips. Fig. 7 shows comparisons of the major strains at the specimen centre L1, and two other locations L2 and L3 which are at distances $D$ = 8 and 16 mm, respectively, from the specimen centre along the length direction. L1, L2, and L3 are

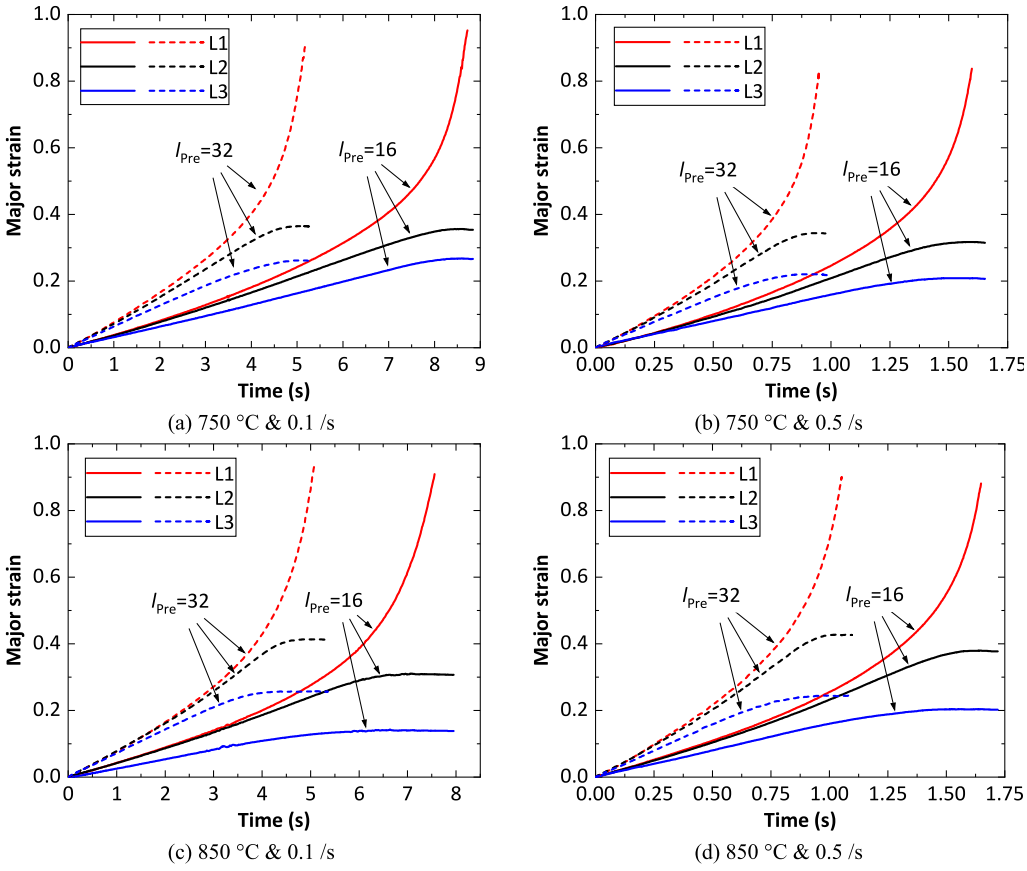


**Fig. 7.** Comparison of major strains (or axial strains) at the locations L1, L2 and L3 which are at a distance ($D$) of 0, 8 and 16 mm, respectively, from the centre of the specimen (Design-I) along the length direction. Two different pre-forming gauge lengths $l_{Pre}$ of 16 and 32 mm were used in these tests on boron steel 22MnB5, and the four different parts of this figure (a)-(d) correspond to different hot stamping conditions.

marked in Fig. 2(a). The strains at L2 and L3 are used to quantitatively show the nonuniformity of the strain distributions, and hence the strain rate distributions along the specimen gauge length. As can be seen in Fig. 7(a), under conditions of 750 °C & 0.1 /s, the strains at L1, L2 and L3 increased at different rates for both $l_{Pre} = 16$ and $l_{Pre} = 32$ mm; the strain at L1 increased dramatically especially in the later stages of deformation, while the strains at L2 and L3 increased more steadily to saturation values. These results are consistent with those presented in Fig. 5. In terms of the effect of $l_{Pre}$, reaching the same strain values at a given location (L1, L2 or L3) took much longer when $l_{Pre} = 16$ mm than when $l_{Pre} = 32$ mm. This indicates that the value of $l_{Pre}$ has a large influence on the strain rates within the gauge area. Similar phenomena can be observed in the tests carried out under other conditions (Figs. 7(b)-(d)).

The strain rates at the locations L1, L2 and L3 were computed throughout the deformation; the results are presented in Fig. 8. As shown in Fig. 8(a), corresponding to test conditions of 750 °C and 0.1 /s, for both $l_{Pre} = 16$ and $l_{Pre} = 32$ mm, the initial strain rates at L1, L2 and L3 were smaller than the target value 0.1 /s. With increasing time, the strain rate at L1 then increased beyond the target value and became higher than the values at L2 and L3. In the later stages of the deformation, the strain rate at L1 soared, while the strain rates at L2 and L3 decreased to zero. The strain rates at L1, L2 and L3 began to diverge from one another from the start of the deformation. It is thus clear that the nonuniformity in strain rate is present from the beginning of deformation and that this is due to the nonuniformity in temperature distribution seen in Fig. 4 rather than to necking. In terms of the effect of $l_{Pre}$, using $l_{Pre} = 32$ mm produced higher strain rates at a given location (L1, L2 or L3) than using $l_{Pre} = 16$ mm. This effect can be further confirmed in Fig. 8(b) in which the strain rate is plotted against the corresponding strain. The same phenomena can also be seen in the tests under other hot stamping conditions (Figs. 8(c)-(h)). It can therefore be concluded that the pre-forming gauge length $l_{Pre}$ has a large influence on the strain rates at different locations along the gauge area, and a higher value of $l_{Pre}$ leads to higher strain rates at a given location.

### 3.2.2. *Stress-strain curves and thermomechanical properties*

Using the data from the tests with $l_{Pre} = 16$ and 32 mm above, the engineering stress-strain curves of 22MnB5 were determined, using the average strain values obtained over a specified post-forming gauge length $l_{Post}$; here, $l_{Post}$ was taken to have the same value as $l_{Pre}$. The $l_{Post}$ value is a virtual value chosen for the interpretation of the test results, and its changes were determined by measuring the distance between two points which were selected based on the strain fields shown in Figs. 5 and 6. The results are shown in Fig. 9. As can be seen in Figs. 9(a)-(d), the shapes of the engineering stress-strain curves of 22MnB5 determined from the thermo-mechanical tests are highly dependent on the value chosen for $l_{Pre}$ for all the conditions investigated. Properties depending on $l_{Pre}$ include, but are not limited to, the yield strength, the ultimate tensile strength (UTS) and the ductility. Specifically, a higher value of $l_{Pre}$ resulted in a higher apparent UTS and a lower apparent ductility for the same test conditions. The higher UTS was attributed to the higher strain rates near the specimen centre, as demonstrated by DIC (Fig. 8).

Fig. 10 presents the values of both the UTS and the ductility to quantify the effect of $l_{Pre}$ on the measured values of these thermo-mechanical properties as determined from the thermo-mechanical tests. As can be seen in Fig. 10(a), for the test conducted at 750 °C & 0.1 /s, the ductility decreased by 28.7%, but the UTS increased by 5.1% when $l_{Pre}$ was increased from 16 mm to 32 mm. Under the other test conditions, the ductility decreased by 29.5% (Fig. 10(b)), 22.6% (Fig. 10

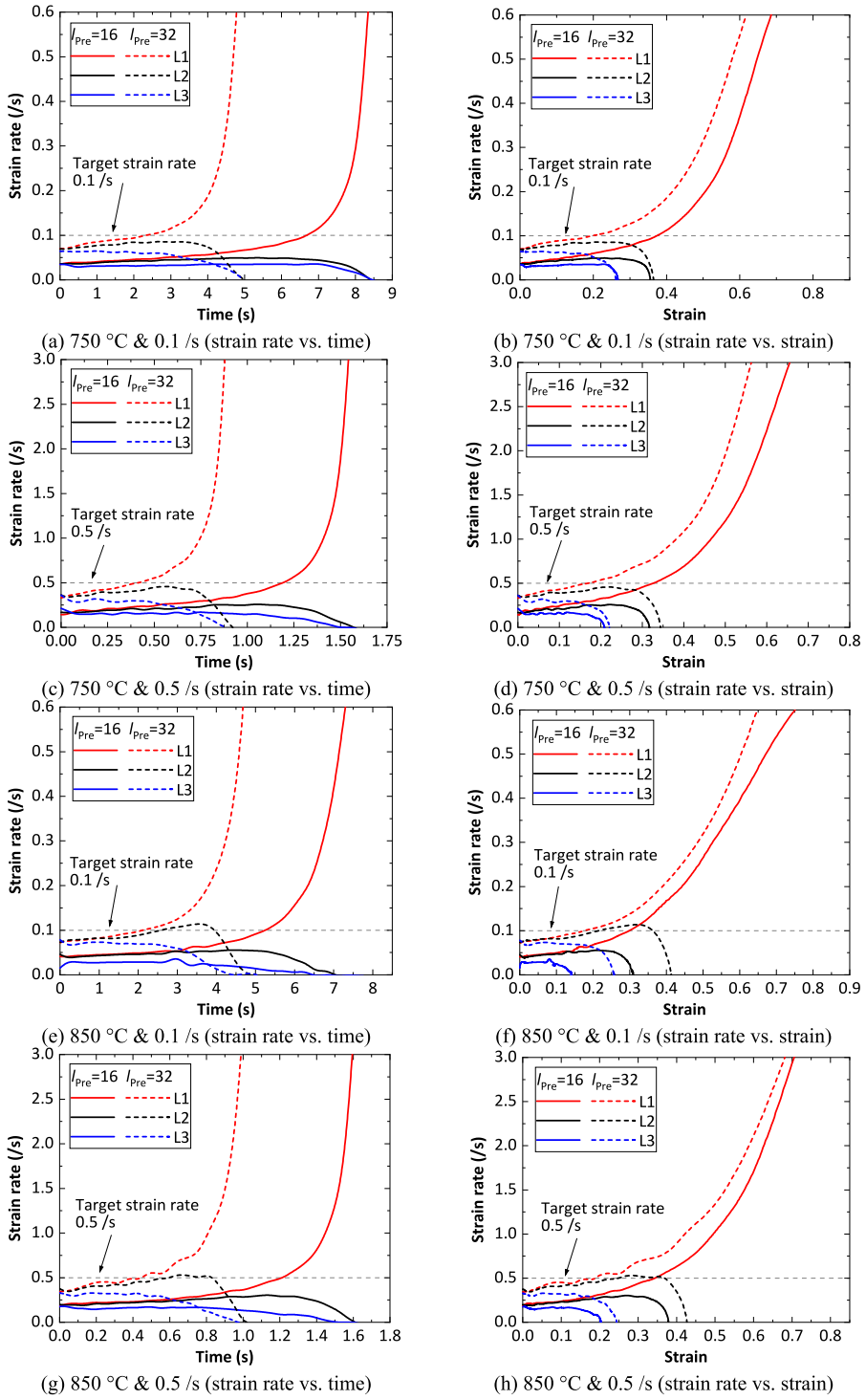


**Fig. 8.** Comparison of strain rates at the locations L1, L2 and L3 which are at distances $D$ = 0, 8 and 16 mm, respectively from the centre of the specimen (Design-I) along the long direction. Two different pre-forming gauge lengths $l_{Pre}$ of 16 and 32 mm were used in these tests on 22MnB5 and different hot stamping conditions were investigated.

(c)), 25.2% (Fig. 10(d)), while the UTS increased by 4.8% (Fig. 10(b)), 6.4% (Fig. 10(c)), 9.1% (Fig. 10(d)). This indicates that the choice of $l_{Pre}$ for the thermo-mechanical tests can cause a large variability in the apparent values of mechanical properties determined from the tests.

### 3.3. Effects of post-forming gauge length $l_{Post}$

#### 3.3.1. Strains and strain rates

In this section, the effect of the post-forming gauge length $l_{Post}$ ($l_{Post} \leq L_0$) on the results of the thermo-mechanical tests was investigated; the $l_{Post}$ value is a virtual value chosen for the interpretation of the test results. For this purpose, five different values of $l_{Post}$ were chosen, namely 4, 8, 16, 24 and 32 mm. Fig. 11 shows the average strains within these gauge lengths throughout deformation in the thermo-mechanical tests for a value $l_{Pre}$ = 32. As can be seen in Fig. 11(a), for testing at 750 °C & 0.1 /s, the strains within the gauge lengths increased steadily with increasing time; these were independent of $l_{Post}$ in early stages, but increasingly diverged at longer times. Specifically, a shorter post-

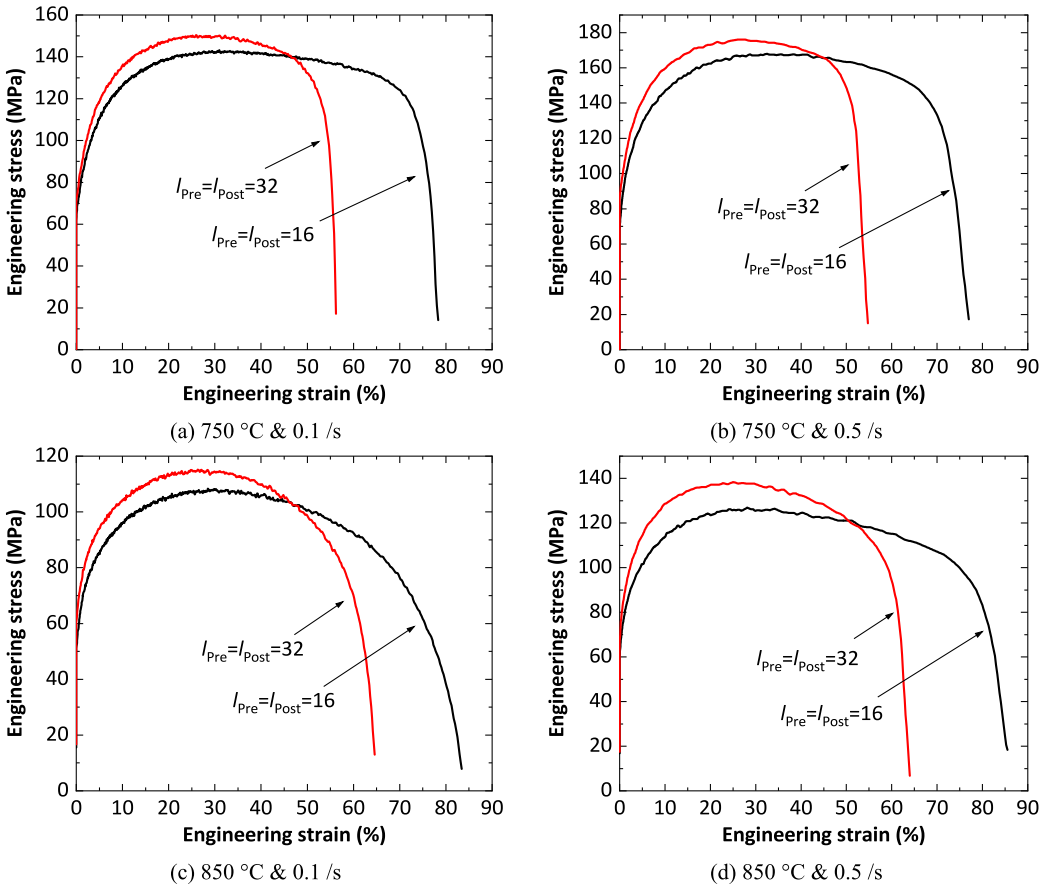


**Fig. 9.** Engineering stress-strain curves for boron steel 22MnB5 determined in tests under different conditions in which two different pre-forming gauge lengths $l_{Pre}$ of 16 and 32 mm were used, and engineering strains were obtained with post-forming gauge lengths $l_{Post}$ having the same values as $l_{Pre}$.

forming gauge length $l_{Post}$ produced higher average strains. This is because of the nonuniformity in strain distributions along the gauge length (Fig. 5), which are attributable to the nonuniformity in the temperature distributions in the earlier stages of deformation. It is worth noting that necking of the material can also contribute to nonuniformity of strain distributions, but this usually only occurs in the later stages of deformation. Similar phenomena can be seen in the results of the tests carried out under the other hot stamping conditions (Figs. 11(b)-(d)).

The average strain rates within the different post-forming gauge lengths $l_{Post}$ were also computed and the results are presented in Fig. 12. As can be seen in Fig. 12(a), for testing at 750 °C & 0.1 /s, the initial strain rates were almost independent of $l_{Post}$, and about 30% lower than the target value of 0.1 /s. With increasing time, the strain rates increased, and similarly to the strains, an increasing divergence appeared between the strain rates as determined with different $l_{Post}$ values; a shorter $l_{Post}$ generated higher strain rates. For example, in the later stages of the deformation, the strain rates determined with $l_{Post}$ = 4 mm soared, while the strain rates for $l_{Post}$ = 32 mm were only slightly higher than the target value. This is consistent with the data presented in Fig. 8, and this divergence among the strain rates is at least partially attributable to the nonuniform temperature distributions, the other possible reason for nonuniformity being necking of samples in the later stages of deformation. The same phenomena can be seen in the results of the tests carried out under the other hot stamping conditions (Figs. 12 (b)-(d)).

### 3.3.2. Stress-strain curves and thermomechanical properties

Using the average strains (Fig. 11) obtained using the different post-forming gauge lengths (i.e. $l_{Post}$ = 4, 8, 16, 24 and 32 mm), the engineering stress-strain curves of 22MnB5 were determined; these are plotted in Fig. 13. As can be seen in Fig. 13(a), corresponding to testing at 750 °C & 0.1 /s, the apparent engineering strains in the stress-strain curves for these different $l_{Post}$ values are different from one another, as would be expected, while the engineering stresses are required to be the same at a given value of time because the stress data are from the same test in each case. Furthermore, the differences in stress-strain curves obtained as a result of modifying $l_{Post}$ are mainly visible in the region beyond UTS only. Similar phenomena can be observed in the results from the tests carried out under the other hot stamping conditions, as shown in Figs. 13(b)-(d).

The engineering stress-strain curves for AA6082 were also obtained using data from the tests where $l_{Pre}$ = 32 mm (as presented in Fig. 6). The average strains obtained using different selected post-forming gauge lengths, i.e. $l_{Post}$ = 5, 10, 20 and 30 mm, were calculated; the results are plotted in Fig. 14. As can be seen in Fig. 14(a) for testing at 375 °C & 0.1 /s, and Fig. 14(b) for testing at 450 °C & 0.5 /s, the shapes of the stress-strain curves are highly dependent on the chosen values of $l_{Post}$, and the curves diverged considerably beyond UTS; these are similar to the observations in the 22MnB5 tests. One main difference from the boron steel is that in AA6082, the UTS appeared very early, almost at the onset of the deformation.

## 3.4. Effects of specimen design

### 3.4.1. Temperature distribution along gauge length

To investigate the effect of specimen design, the temperature distributions along the gauge length of the specimens with Design-II and Design-III were measured. The results are plotted in Fig. 15. As can be seen in Figs. 15(a)-(b), the temperature decreased with increasing distance from the specimen centre as expected. Compared to Design-I

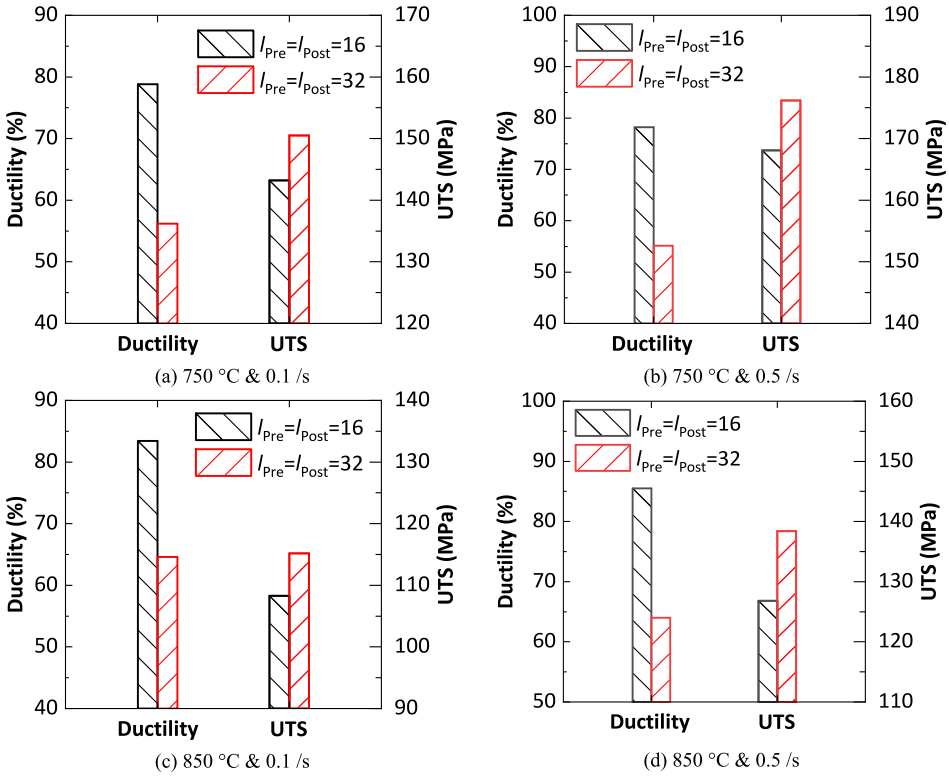


**Fig. 10.** Investigation of the effect of different pre-forming gauge lengths $l_{Pre}$ of 16 and 32 mm on apparent values of ductility and UTS of 22MnB5 as determined in tests under different conditions; the ductility was obtained assuming a post-forming gauge length $l_{Post}$ with the same value as $l_{Pre}$.

(Fig. 4(a)), larger temperature drops can be observed in Design-II (Fig. 15(a)) at locations having the same distance from the specimen centre. This is because the initial length $L_0$ of the gauge area of Design-II is 50% shorter than that of Design-I. It is therefore concluded that a longer $L_0$ is beneficial to produce more uniform temperature fields in a central gauge region of the same fixed length. In addition, compared to Design-II (Fig. 15(a)), larger temperature drops can be seen in Design-III (Fig. 15(b)). The only difference between Design-II and Design-III is that the initial width $W_0$ of the gauge area of the latter is 50% less than that of the former. This indicates that $W_0$ also has an influence on the temperature distributions, and a wider $W_0$ enables more uniform temperature distributions to be produced in a central gauge region of the same length.

### 3.4.2. Strains and strain rates

Using the specimens with Design-II and Design-III, thermo-mechanical tests on 22MnB5 were carried out under the hot stamping conditions given in Table 1. The same pre-forming gauge length $l_{Pre}$ = 16 mm was used for all these tests. The strains at the locations L1 ($D$ = 0 mm) and L2 ($D$ = 8 mm) in Design-II and Design-III were computed throughout deformation, where $D$ is the distance from the specimen centre along the long direction. The resulting strains are plotted in Fig. 16, with those from Design-I included for comparison. As can be seen in Fig. 16(a), for testing at 750 °C & 0.1 /s, the strain at L1 (i.e. the specimen centre) increased considerably, especially in the later stages of deformation in both Design-II and Design-III, while the strain at L2 increased before reaching saturation values in both designs. These trends are similar to those observed for the strains in Design-I. Both alternative designs took a much shorter time to fracture than Design-I; if $t_F$ is defined as the time to fracture for Design-I, then Design-II fractured at about 0.49$t_F$ and Design-III fractured at about 0.45$t_F$. In addition, the strains at L1 at the time of fracture in both Design-II and Design-III were lower than that in Design-I. The same phenomena can also be seen in the results of the tests performed under the other hot stamping conditions, as shown in Figs. 16 (b)-(d).

The strain rates at L1 (i.e. the specimen centre) and L2 in Design-II and Design-III were computed and compared with those in Design-I, and the results are plotted in Fig. 17. It can be seen from Fig. 17(a) that, for testing at 750 °C & 0.1 /s, the strain rates at L1 increased dramatically in the later stages of deformation in both Design-II and Design-III. However, in contrast to those in Design-I, the strain rates at L1 in both Design-II and Design-III were much higher than those at L2 even in the initial stages of deformation. This is because the temperature distributions in Design-II and Design-III were less uniform than those in Design-I, as demonstrated in Figs. 4 and 15. Furthermore, the strain rates at L1 in Design-II in the initial stages of deformation were much higher than those in Design-I, but slightly lower than those in Design-III. This can be further confirmed by Fig. 16(b) which shows the strain rates at L1 plotted against the corresponding strains. The same phenomena can also be seen in the results from tests performed under the other hot stamping conditions, as shown in Figs. 17(b)-(h). Overall, the observations above indicate that both the length $L_0$ and width $W_0$ of the gauge area of the specimens affect the distributions and numerical values of the strain rates. Specifically, a longer $L_0$ produces strain rate distributions that are more uniform in a gauge region of the same length, but smaller strain rate values in the initial stages of deformation. A wider $W_0$ produces higher strain rate values at a given location.

### 3.4.3. Stress-strain curves and thermomechanical properties

Using the data from the tests on Design-II and Design-III above, the engineering stress-strain curves of 22MnB5 were determined with a post-forming gauge length $l_{Post}$ = 16 mm equal to $l_{Pre}$. The resulting stress-strain curves obtained using Design-II and Design-III are plotted in Fig. 18, together with those obtained using Design-I for comparison. As can be seen in Fig. 18(a), for the test conducted at 750 °C & 0.1 /s, different forms of stress-strain curves were obtained when using the different specimen designs; parameters whose measured values are different include the UTS and the ductility. Specifically, the UTS

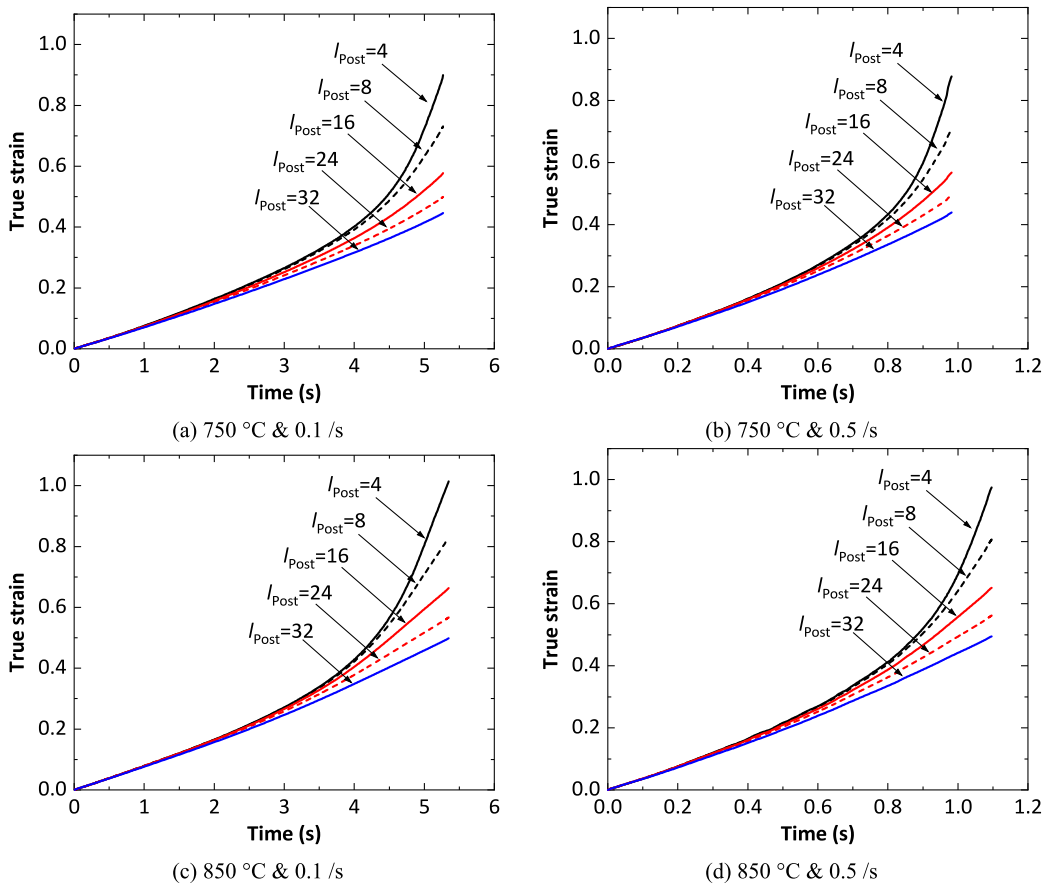


**Fig. 11.** Evolution of apparent true strains within different selected post-forming gauge lengths ($l_{Post}$) of 4, 8, 16, 24 and 32 mm in tests on 22MnB5 under different test conditions. All the tests were performed using a pre-forming gauge length $l_{Pre}$ of 32 mm.

measured using Design-II was about 11% higher than that using Design-I, while the value obtained using Design-III was about 17% higher than for Design-I. The ductility values obtained using Design-II and Design-III were very similar, but much smaller (about 35% smaller) than that using Design-I. In the tests carried out under the other hot stamping conditions, similar effects of the specimen design on these thermomechanical properties can be seen (Fig. 18(b)). It is therefore concluded that the specimen design, specifically the initial length $L_0$ and width $W_0$, strongly affects the engineering stress-strain curves and the UTS and ductility values obtained from them.

### 3.5. *Distribution of microstructural features in the gauge length – A case study*

The nonuniform temperature distributions (Figs. 4 and 15) may affect the distributions of microstructural features and properties (e.g. geometrically necessary dislocation (GND) density, grain size and phase fractions and sizes) along the gauge length by influencing the kinetics of phenomena including but not limited to recovery, recrystallisation and phase transformation. A case study was carried out, as an example, on a 22MnB5 specimen with Design-I. A hot stamping heat treatment was carried out, in which, as illustrated in Fig. 3(b), the material was heated to 925 °C followed by soaking for 60 s with the aim of achieving complete transformation from ferrite to austenite, and then rapidly quenched at a rate of 60 °C/s to room temperature. The microstructure of the specimen at four locations L1, L2, L3, L4 at distances $D$ from the centre of 0, 8, 16, 24 mm respectively, was characterised. The results are shown in Fig. 19. As can be seen in Figs. 19(a)-(b), the material at L1 and L2 was fully transformed to martensite, indicating that full austenitisation had occurred before quenching [36]. However, at locations L3 and L4, as shown in Figs. 19(c)-(d), residual ferrite can be seen, with a greater proportion of such ferrite at L4 ($D$ = 24 mm) than at L3 ($D$ = 16 mm). This indicates that, due to the temperature decrease along the gauge length, full austenitisation was not achieved at L3 and L4. It can therefore be concluded that, to investigate the microstructure produced during the thermo-mechanical tests, the location used for characterisation of the microstructural features should be as close as possible to the specimen centre due to the nonuniform temperature distributions. It should be noted that the microstructure of AA6082 was not investigated in the present study because this case study of boron steel is sufficient to support that nonuniform temperature distributions along the gauge length could result in nonuniform microstructure distributions.

## 4. Discussion

For thermo-mechanical testing at high temperatures, it is essential to accurately control both the temperature and the strain rate in the gauge length throughout the deformation [37]. In the tests conducted using the Gleeble system, the temperature distributions along the gauge length are nonuniform and the temperature is highest at the specimen centre, as shown in Figs. 4 and 15. In addition, only the temperature at one given location (namely the specimen centre in the present study) can be controlled accurately. The nonuniform temperature distributions lead to a concomitant nonuniformity of strains (Fig. 7) and strain rates (Fig. 8) along the gauge length; both strains and strain rates are highest at the specimen centre. Therefore, control of the displacement of the specimen grips used to stretch specimens can directly control only the strain rates at the specimen centre; the strain rates elsewhere in the specimen are controlled indirectly. In summary, in the tests performed in the Gleeble, both the temperature and the strain rate are nonuniformly distributed

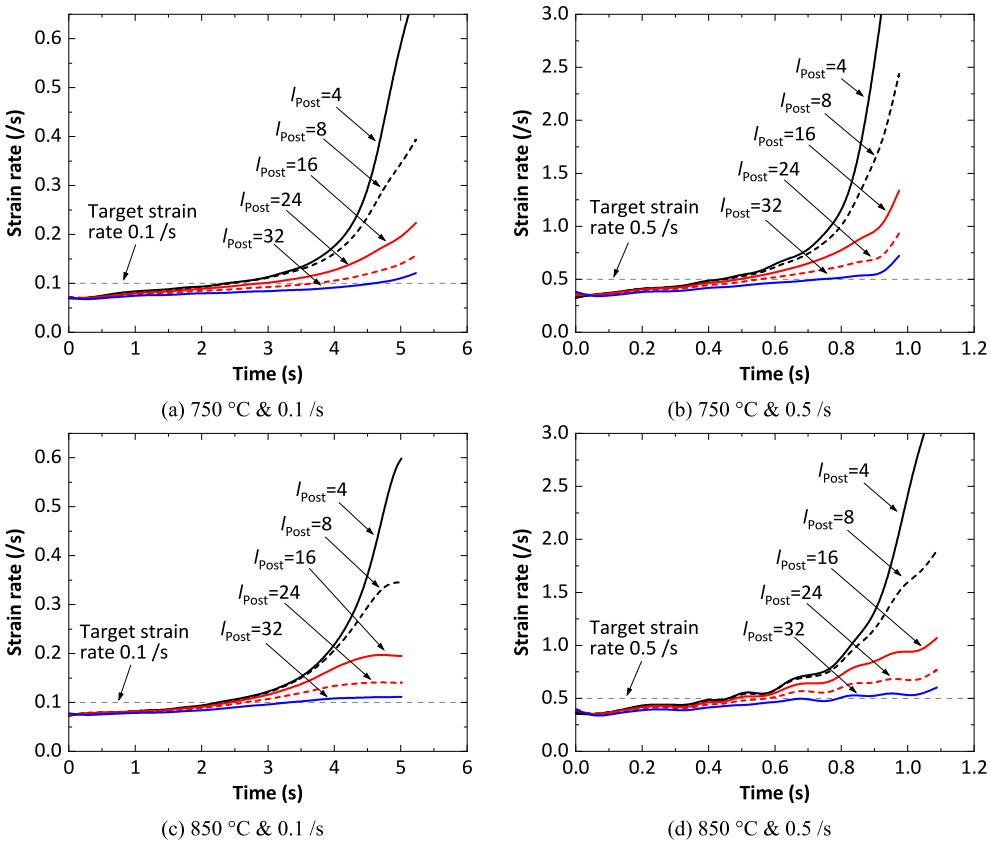


**Fig. 12.** Evolution of average strain rates with different selected post-forming gauge lengths ($l_{Post}$) of 4, 8, 16, 24 and 32 mm in tests on 22MnB5 under different conditions. All the tests were performed using a pre-forming gauge length $l_{Pre}$ of 32 mm.

along the gauge length, and these parameters can only be controlled directly at the specimen centre where their values are the highest.

As a result of the nonuniformity of the deformation along the gauge length, it is difficult to control the practical values of the strain rates in the gauge area to obtain target values. In the present study, Eq. (1) was used to calculate the displacement of the specimen grips required to stretch the specimens for the attainment of the target strain rates. However, the use of this equation is based on the assumption that the deformation in the gauge area is uniform, which is not the case in tests using the Gleeble even in the early stages of deformation. Indeed, according to Fig. 8, the value chosen for the pre-forming gauge length $l_{Pre}$ in this equation significantly affects the actual strain rates in the gauge area; the higher $l_{Pre}$, the higher the strain rates at a given location. In practice, the strain rates are not constant with respect to time, but change continuously from the beginning of the deformation, with values at different locations in the gauge area changing in different ways. This indicates that the target strain rates cannot be obtained at any location (e.g. the specimen centre) in the gauge area simply by using Eq. (1) to determine the displacement required to stretch the specimens. To achieve the target strain rates, Eq. (1) needs to be improved by taking into account the nonuniformity of temperature distributions along the gauge length in the calculation. According to Figs. 4 and 15, the temperature distributions are dependent on the material and the specimen dimensions, namely the length and width of the gauge area. Therefore, an improved version of Eq. (1) would probably need to consider the material and the specimen dimensions.

The nonuniformity of the distributions of temperature and strain rate along the gauge length results in variability in the apparent values of materials properties under a given set of test conditions, such as the ductility and the UTS, depending on the parameters used in the thermo-mechanical tests and the interpretation of their results. According to Figs. 13 and 14, the apparent ductility obtained depends strongly on the post-forming gauge length; the longer the $l_{Post}$, the lower the ductility. This is because of the nonuniform deformation along the gauge length which is in turn caused by the nonuniform temperature distributions [38] and the occurrence of necking [39]. For testing at room temperature, an initial sample gauge length $L_0$ which is 4 to 6 times the initial width $W_0$ of the gauge area is usually recommended to minimise the effect of the nonuniformities in deformation caused by necking on the ductility measured within the gauge length [40]. However, the present study has shown that this rule for selection of an appropriate gauge length is not applicable to thermo-mechanical testing. This is because nonuniform deformation already starts at the beginning of the test due to the nonuniformity of the temperature distribution. Given that the strain distributions within the same gauge length are dependent on the pre-forming gauge length $l_{Pre}$ (Fig. 7) and the specimen dimensions (Fig. 16), the ductility value obtained using the thermo-mechanical tests is therefore relative and dependent on $l_{Pre}$, $l_{Post}$ and the specimen dimensions (i.e. the initial length $L_0$ and width $W_0$ of the gauge area). The measured UTS is, according to Figs. 9 and 18, dependent on $l_{Pre}$ and the specimen dimensions $L_0$ and $W_0$. Considering that the specimen centre has the highest deformation and fracture occurs at this location, the UTS is the maximum stress that the material at the specimen centre can withstand while being stretched. The strain rates at the specimen centre depend on $l_{Pre}$ (Fig. 8), $L_0$ and $W_0$ (Figs. 17), giving rise to the observed variabilities in the UTS value measured in thermo-mechanical testing.

Furthermore, it is challenging to determine true stress–true strain curves for sheet metals subjected to thermo-mechanical tests in the Gleeble. Usually, a true stress–strain curve is valid only while deformation is uniform, due to the effects of nonuniform deformation (e.g. necking) on the calculation of true stresses [41]. In the thermo-mechanical tests in the present work, however, the deformation is nonuniform from the beginning of testing (Figs. 5 and 6). One may consider that, similarly to testing at room temperature, the true

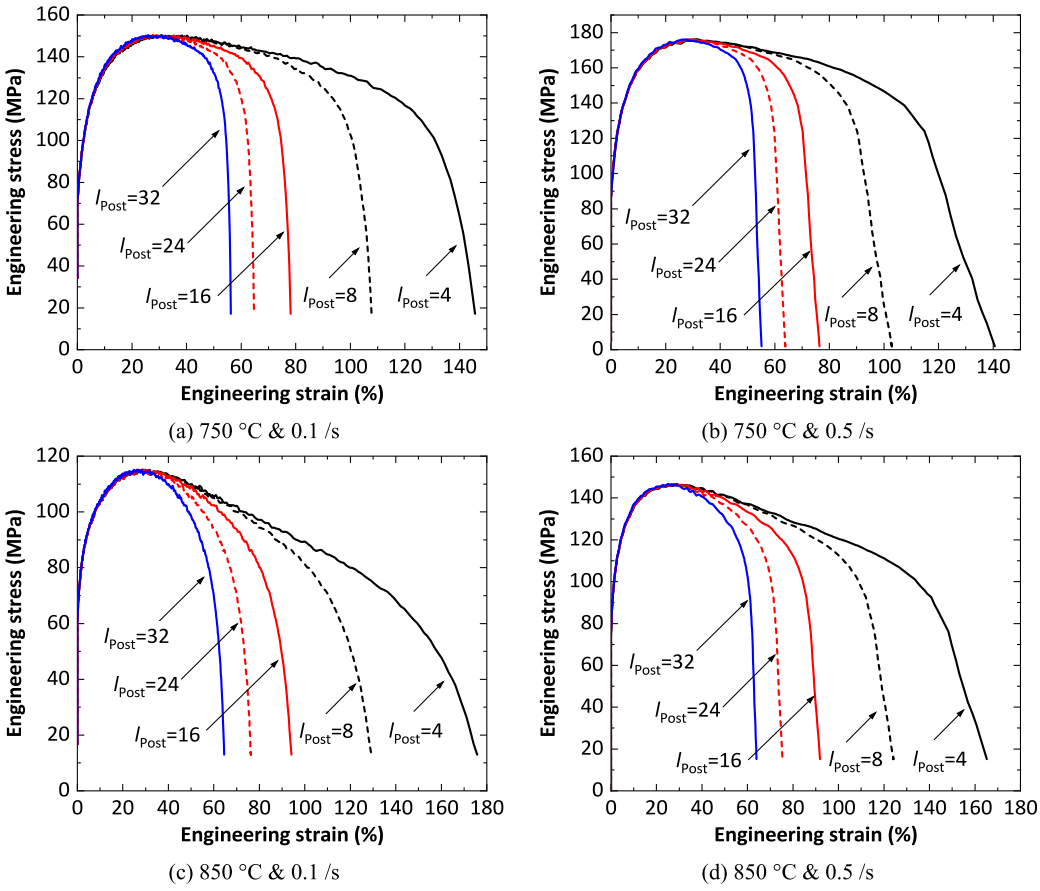


**Fig. 13.** Engineering stress-strain curves obtained using different post-forming gauge length $l_{Post}$ values of 4, 8, 16, 24, 32 mm in tests on 22MnB5 under different conditions. All the tests were performed using a pre-forming gauge length $l_{Pre}$ of 32 mm.

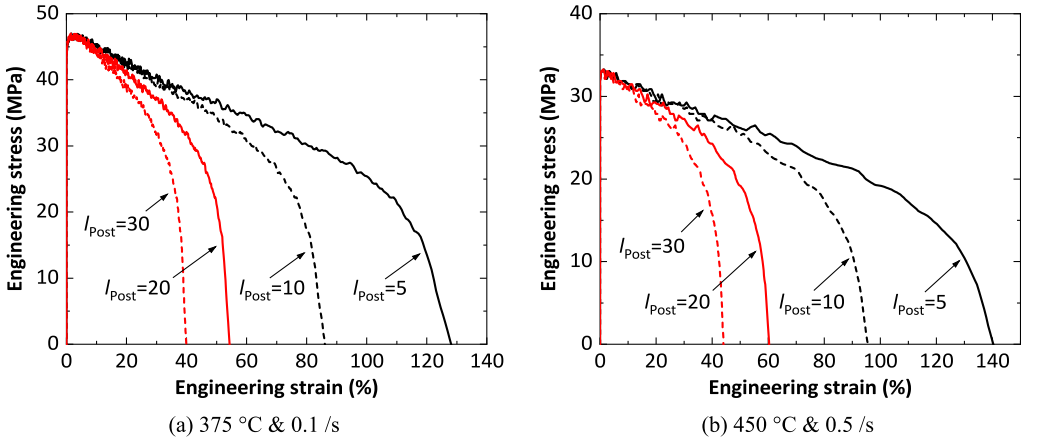


**Fig. 14.** Engineering stress-strain curves obtained using different post-forming gauge length ($l_{Post}$) values of 5, 10, 20 and 30 mm in tests on AA6082 under different test conditions. All the tests were performed using a pre-forming gauge length $l_{Pre}$ of 16 mm.

stress–true strain curves could be determined using the test data from the part of the curve before the maximum of engineering stress (i.e. the UTS) is reached. However, the form of the resulting curves would still be dependent on the pre-forming gauge length $l_{Pre}$, the post forming gauge length $l_{Post}$, and the specimen design. In addition, for AA6082 (Fig. 14), the total true strain would be very small (e.g. 0.03) because the UTS occurs almost at the beginning of the deformation, indicating that the specimen Design-I and the data post-processing method used are for AA6082 not adapted particularly. Therefore, a standard method needs to be developed in future to determine unique true stress–true strain curves for sheet metals at high temperatures.

It should be noted that the dependencies on experimental parameters investigated in the present study are not restricted to high-temperature testing in the Gleeble, but would apply to any tests in which temperature distributions along the gauge length are nonuniform, especially when the total deformation is relatively high [42].

## 5. Conclusions

In thermo-mechanical tests where temperature distributions along

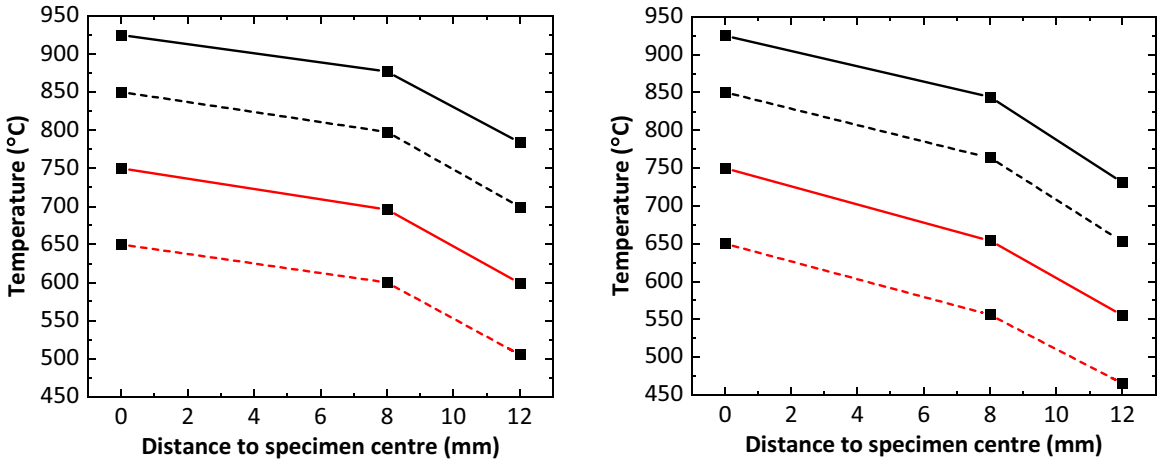


**Fig. 15.** Temperature distributions along the length direction of the 22MnB5 specimens with different designs, Design-II and Design-III, for tests in which the temperature at the specimen centre reaches target values of 650, 750, 850 and 925 °C.

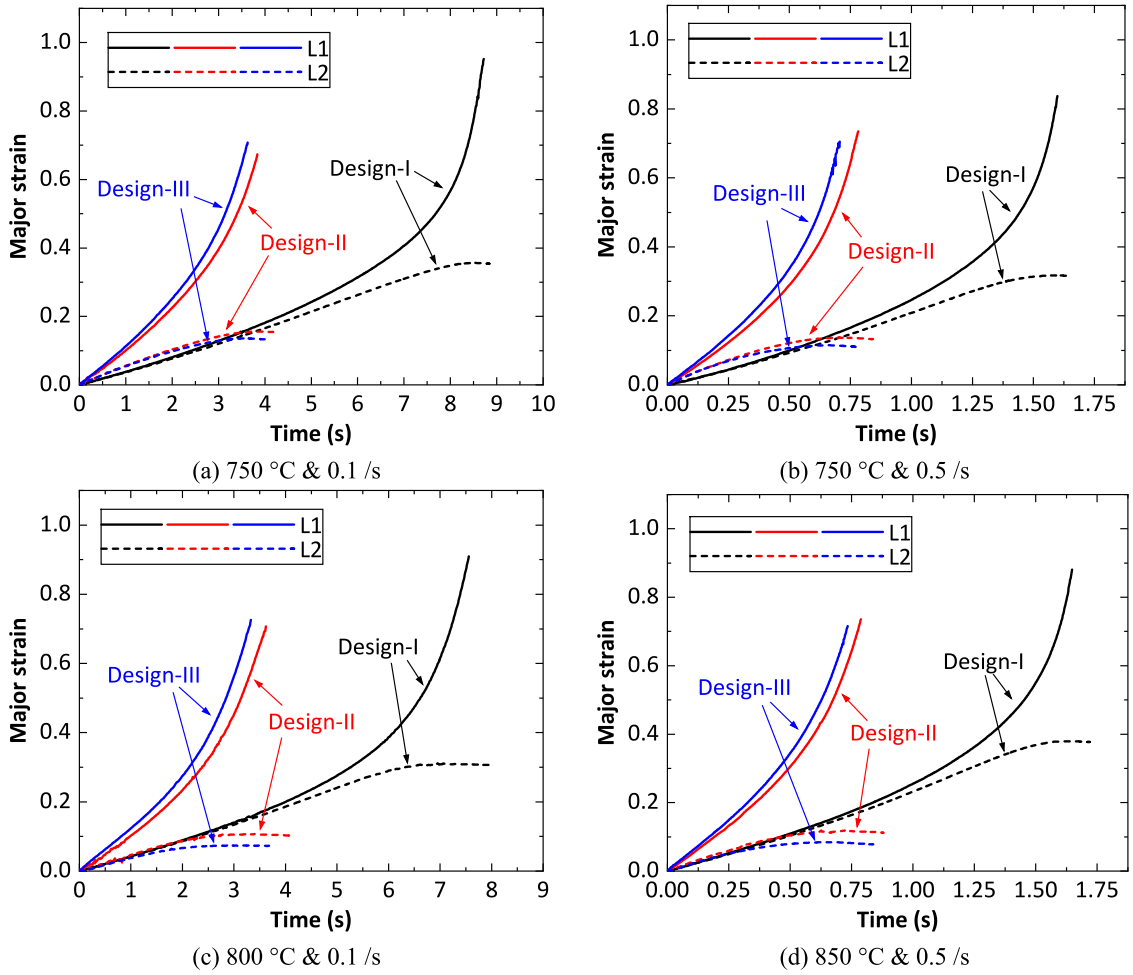


**Fig. 16.** Major strains (or axial strains) at the locations L1 and L2 which are at a distance $D = 0$ and 8 mm respectively from the centre along the long axis of the specimens, plotted for the different designs: Design-I, Design-II and Design-III, in the tests on 22MnB5 under different hot stamping conditions using $l_{Pre} = 16$ mm.

the gauge length are nonuniform throughout the deformation due to heat loss to the specimen grips, these temperature distributions lead to nonuniformity in the distributions of both strain and strain rate. The strain and strain rate have their highest values at the specimen centre where the temperature is highest, and decrease with increasing distance from the specimen centre. In a case study, the temperature distributions were found to result in nonuniformities in the microstructure along the gauge length.

Since the strain and strain rate along the gauge length are nonuniform, the apparent values of mechanical properties of sheet metals, such

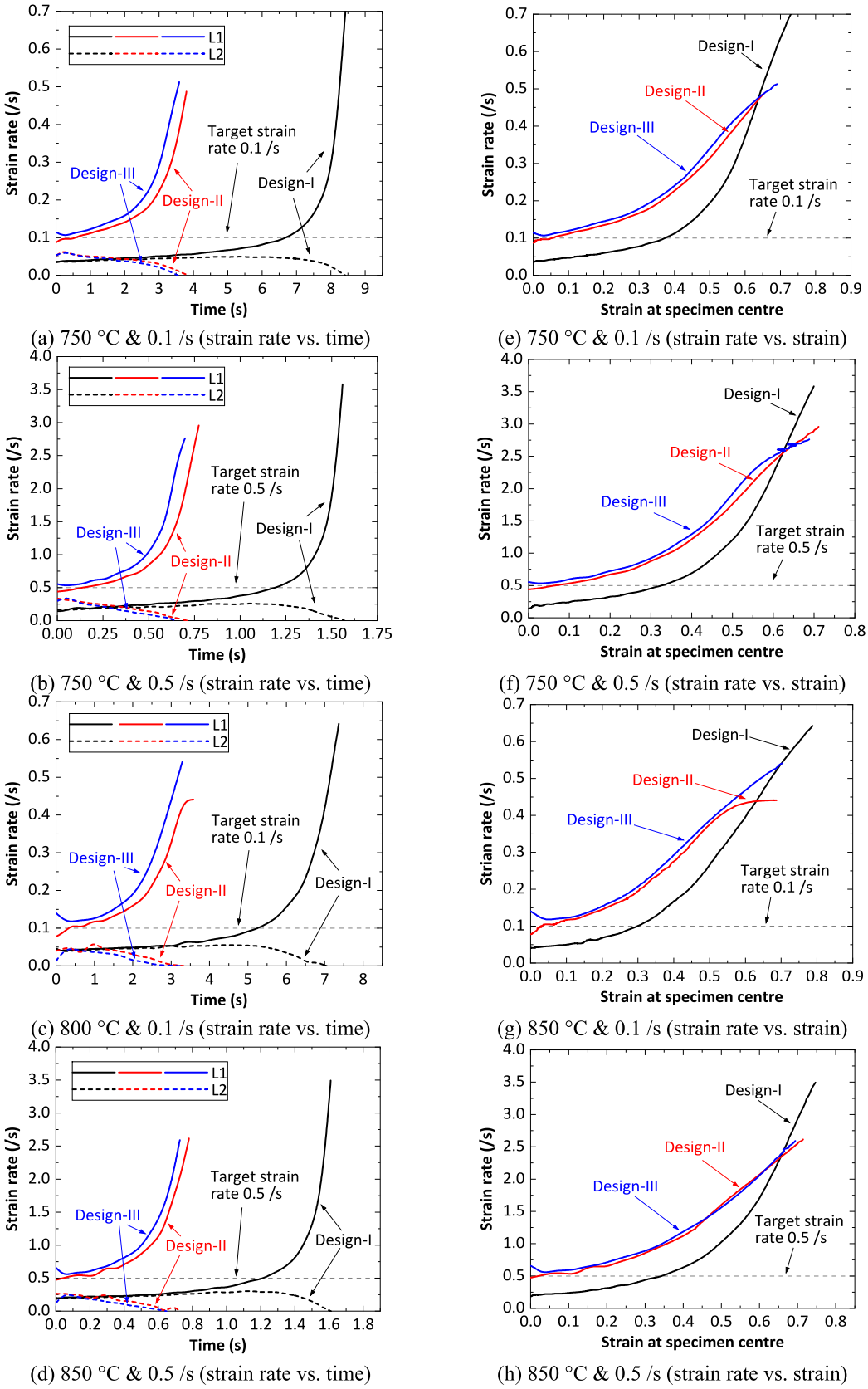


**Fig. 17.** Evolution of strain rates at the locations L1 and L2 that are at a distance $D = 0$ and 8 mm respectively, from the centre along the long direction, in the specimens with the different designs: Design-I, Design-II and Design-III, in the tests for 22MnB5 under different hot stamping conditions using $l_{Pre} = 16$ mm. Note that in (e)-(h) only the strain rates at the specimen centre are plotted.

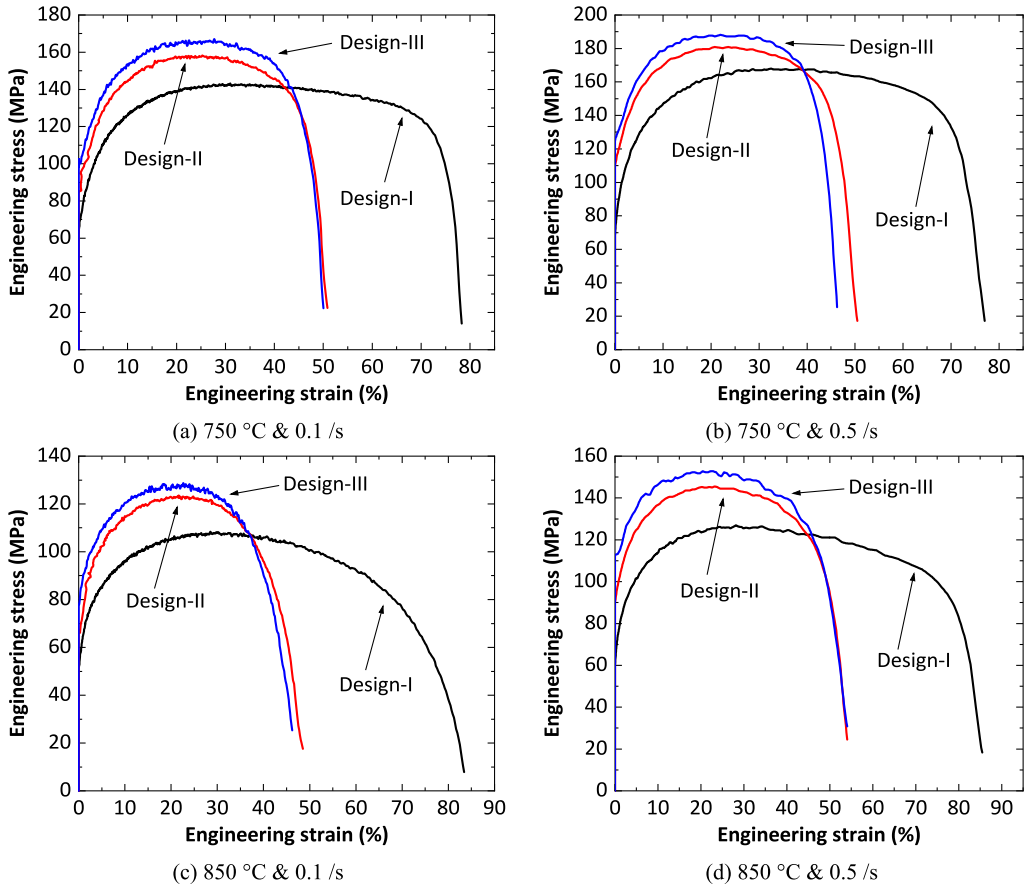


**Fig. 18.** Engineering stress-strain curves obtained using specimens with different designs, Design-I, Design-II and Design-III in tests on 22MnB5 under hot stamping different conditions in which the pre-forming and post-forming gauge lengths were set to the same value $l_{Pre} = l_{Post} = 16$ mm.

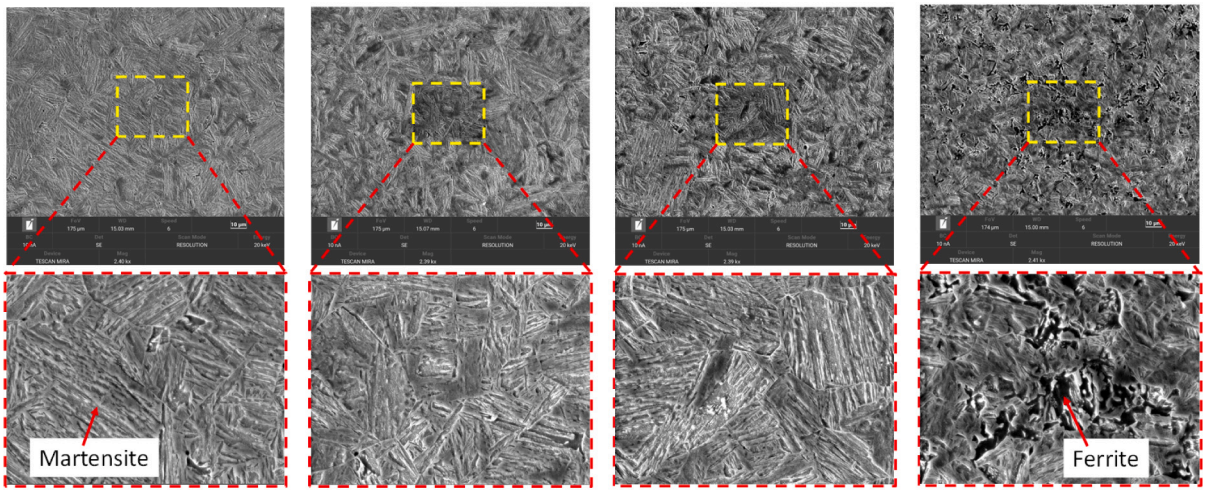


**Fig. 19.** Microstructure distributions along the length direction of a boron steel specimen (Design-I) after the hot stamping thermal cycle, showing four locations at distances ($D$) of 0, 8, 16 and 24 mm from the specimen centre.

as the ductility and the ultimate tensile strength (UTS), as determined from the thermo-mechanical tests depend strongly on the pre-forming gauge length $l_{Pre}$, the post forming gauge length $l_{Post}$, and the specimen design. Specifically: 1) The value of $l_{Pre}$ determines the displacements required to stretch specimens directly, and thus affects the strain rates in the gauge area. A higher $l_{Pre}$ results in higher strain rates applied to the gauge area. For the same specimen design, and setting $l_{Post} = l_{Pre}$, a higher UTS and a lower ductility are obtained. 2) Decreasing the $l_{Post}$ value increases both the average strain and average strain rate within the gauge length, especially in the later stages of each test. The $l_{Post}$ value has only a small effect on the UTS, but affects the ductility characterised from the test considerably; the higher $l_{Post}$, the lower the ductility. 3) In terms of the effects of the specimen design, only the initial length $L_0$ and width $W_0$ of the gauge area were investigated in the present study. A

smaller $L_0$ leads to a decrease in the strain rates and the ductility, but an increase in the UTS. In contrast, decreasing $W_0$ increases the strain rates and the UTS, but has only a small effect on the ductility.

Due to the uncertainties mentioned above, it is very challenging to characterise absolute materials properties, such as UTS and ductility, from these thermo-mechanical tests using the Gleeble, because the specimens are subjected to nonuniform temperature distributions along the gauge length. Further work is required to develop methods to obtain target strain rates and to determine true stress–true strain curves with these test methods.

## Abbreviations

| | |
|---|---|
| UTS | Ultimate Tensile Strength |
| DIC | Digital Image Correlation |
| SHT | Solution Heat Treatment |
| fps | frames per second |
| SEM | Scanning Electron Microscope |
| GND | Geometrically Necessary Dislocation |

## Declaration of competing interest

The authors declare that they have no known competing financial interests or personal relationships that could have appeared to influence the work reported in this paper.

## Acknowledgements

This work was supported by the Engineering and Physical Sciences Research Council (EPSRC) [Grant number EP/R001715/1] on “Lightform: Embedding Materials Engineering in Manufacturing with Light Alloys”.

## References

[1] Taylor T, Clough A. Critical review of automotive hot-stamped sheet steel from an industrial perspective. Mater. Sci. Technol. 2018;34:809–61. https://doi.org/10.1080/02670836.2018.1425239.
[2] Wilson DV. Aluminium versus steel in the family car — the formability factor. J. Mech. Work. Technol. 1988. https://doi.org/10.1016/0378-3804(88)90055-1.
[3] Chen Z, Fang G, Zhao J-Q. Formability evaluation of aluminum alloy 6061-T6 sheet at room and elevated temperatures. J. Mater. Eng. Perform. 2017;26:4626–37. https://doi.org/10.1007/s11665-017-2895-0.
[4] Bong HJ, Barlat F, Ahn DC, Kim H-Y, Lee M-G. Formability of austenitic and ferritic stainless steels at warm forming temperature. Int. J. Mech. Sci. 2013;75:94–109. https://doi.org/10.1016/j.ijmecsci.2013.05.017.
[5] ASTM International. Standard test methods for tension testing of metallic materials, ASTM international, West Conshohocken. PA 2016. https://doi.org/10.1520/E0008_E0008M-16AE01.
[6] ASTM International. Standard test methods for elevated temperature tension tests of metallic materials, ASTM. International 2009;E21-09. https://doi.org/10.1520/E0021-20.
[7] Alhammadi A, Al-Ketan O, Khan KA, Ali M, Rowshan R, Abu Al-Rub RK. Microstructural characterization and thermomechanical behavior of additively manufactured AlSi10Mg sheet cellular materials. Mater. Sci. Eng. A 2020;791. https://doi.org/10.1016/j.msea.2020.139714.
[8] Gui Z, Liang W, Liu Y, Zhang Y. Thermo-mechanical behavior of the Al–Si alloy coated hot stamping boron steel. Mater. Des. 2014;60:26–33. https://doi.org/10.1016/j.matdes.2014.03.011.
[9] Zhang C, Chu X, Guines D, Leotoing L, Ding J, Zhao G. Dedicated linear–voce model and its application in investigating temperature and strain rate effects on sheet formability of aluminum alloys. Mater. Des. 2015;67:522–30. https://doi.org/10.1016/j.matdes.2014.10.074.
[10] Valeri G, Koohbor B, Kidane A, Sutton MA. Determining the tensile response of materials at high temperature using DIC and the Virtual Fields Method. Opt. Lasers Eng. 2017;91:53–61. https://doi.org/10.1016/j.optlaseng.2016.11.004.
[11] Ying L, Gao T, Rong H, Han X, Hu P, Hou W. On the thermal forming limit diagram (TFLD) with GTN mesoscopic damage model for AA7075 aluminum alloy: numerical and experimental investigation. J. Alloys Compd. 2019;802:675–93. https://doi.org/10.1016/j.jallcom.2019.05.342.
[12] Jenner F, Walter ME, Iyengar RM, Hughes RL. Application of high-speed video extensometry for high-temperature tensile characterization of boron heat-treated steels, The. J. Strain Anal. Eng. Des. 2014;49:378–87.
[13] Merklein M, Lechler J. Investigation of the thermo-mechanical properties of hot stamping steels. J. Mater. Process. Technol. 2006;177:452–5. https://doi.org/10.1016/j.jmatprotec.2006.03.233.
[14] Min J, Lin J, Min YA. Effect of thermo-mechanical process on the microstructure and secondary-deformation behavior of 22MnB5 steels. J. Mater. Process. Technol. 2013;213:818–25.
[15] Liu Y, Zhu Z, Wang Z, Zhu B, Wang Y, Zhang Y. Flow and friction behaviors of 6061 aluminum alloy at elevated temperatures and hot stamping of a B-pillar. Int. J. Adv. Manuf. Technol. 2018;96:4063–83. https://doi.org/10.1007/s00170-018-1790-7.
[16] Karbasian H, Tekkaya AE. A review on hot stamping. J. Mater. Process. Technol. 2010;210:2103–18. https://doi.org/10.1016/j.jmatprotec.2010.07.019.
[17] Thermal-Mechanical Physical Simulation System. https://www.gleeble.com/products/gleeble-systems/gleeble-3800.html. Accessed 15/08 2022.
[18] Abspoel M, Neelis BM, van Liempt P. Constitutive behaviour under hot stamping conditions. J. Mater. Process. Technol. 2016;228:34–42. https://doi.org/10.1016/j.jmatprotec.2015.05.007.
[19] Li Y, Li S, Chen Y, Han G. Constitutive parameters identification based on DIC assisted thermo-mechanical tensile test for hot stamping of boron steel. J. Mater. Process. Technol. 2019;271:429–43. https://doi.org/10.1016/j.jmatprotec.2019.04.020.
[20] Martins JMP, Thuillier S, Andrade-Campos A. Calibration of a modified Johnson-Cook model using the Virtual Fields Method and a heterogeneous thermo-mechanical tensile test. Int. J. Mech. Sci. 2021;202-203. https://doi.org/10.1016/j.ijmecsci.2021.106511.
[21] Coër J, Bernard C, Laurent H, Andrade-Campos A, Thuillier S. The effect of temperature on anisotropy properties of an aluminium alloy. Exp. Mech. 2010;51:1185–95. https://doi.org/10.1007/s11340-010-9415-6.
[22] Ganapathy M, Li N, Lin J, Abspoel M, Bhattacharjee D. A novel grip design for high-accuracy thermo-mechanical tensile testing of boron steel under hot stamping conditions. Exp. Mech. 2018;58:243–58. https://doi.org/10.1007/s11340-017-0333-8.
[23] Shi D, Hu P, Ying L. Comparative study of ductile fracture prediction of 22MnB5 steel in hot stamping process. Int. J. Adv. Manuf. Technol. 2015. https://doi.org/10.1007/s00170-015-7754-2.
[24] Cullen GW, Korkolis YP. Ductility of 304 stainless steel under pulsed uniaxial loading. Int. J. Solids Struct. 2013;50:1621–33. https://doi.org/10.1016/j.ijsolstr.2013.01.020.
[25] Zou DQ, Li SH, He J. Temperature and strain rate dependent deformation induced martensitic transformation and flow behavior of quenching and partitioning steels. Mater. Sci. Eng. A 2017;680:54–63. https://doi.org/10.1016/j.msea.2016.10.083.
[26] Admin (2015) Induction Forge: Video Shows The Induction Heating In Action. https://www.technocrazed.com/induction-forge-interesting-video-shows-the-induction-heating-in-action. Accessed 01/02/2023.
[27] High Temperature Test Furances. https://retrofitmach.com/category5-high-temperature-test-furnaces.html. Accessed 01/02/2023.
[28] Introducing the Gleeble 500 Series: An Economical Platform for Metallurgy Research https://www.gleeble.com/500-series.html. Accessed 01/02/2023.
[29] Kardoulaki E, Lin J, Balint D, Farrugia D. Investigation of the effects of thermal gradients present in Gleeble high-temperature tensile tests on the strain state for free cutting steel, The. J. Strain Anal. Eng. Des. 2014;49:521–32. https://doi.org/10.1177/0309324714531950.
[30] Shao Z, Li N, Lin J, Dean TA. Strain measurement and error analysis in thermo-mechanical tensile tests of sheet metals for hot stamping applications. Proc. Inst. Mech. Eng. C J. Mech. Eng. Sci. 2018;232:1994–2008. https://doi.org/10.1177/0954406217714011.
[31] Zhang R, Shao Z, Lin J, Dean TA. Measurement and analysis of heterogeneous strain fields in uniaxial tensile tests for boron steel under hot stamping conditions. Exp. Mech. 2020;60:1289–300. https://doi.org/10.1007/s11340-020-00658-6.
[32] Zhang R, Shi Z, Yardley VA, Lin J. Experimental studies of necking and fracture limits of boron steel sheet under hot stamping conditions. J. Mater. Process. Technol. 2022;302. https://doi.org/10.1016/j.jmatprotec.2021.117481.
[33] Shao Z, Li N, Lin J, Dean T. Formability evaluation for sheet metals under hot stamping conditions by a novel biaxial testing system and a new materials model. Int. J. Mech. Sci. 2017;120:149–58. https://doi.org/10.1016/j.ijmecsci.2016.11.022.
[34] Tong C, Rong Q, Yardley VA, Shi Z, Li X, Zhang B, et al. Investigation of deformation behaviour with yield point phenomenon in cold-rolled medium-Mn steel under hot stamping conditions. J. Mater. Process. Technol. 2022;306. https://doi.org/10.1016/j.jmatprotec.2022.117623.
[35] Khan AA. Electrode wear and material removal rate during EDM of aluminum and mild steel using copper and brass electrodes. Int. J. Adv. Manuf. Technol. 2007;39:482–7. https://doi.org/10.1007/s00170-007-1241-3.
[36] Merklein M, Wieland M, Lechner M, Bruschi S, Ghiotti A. Hot stamping of boron steel sheets with tailored properties: a review. J. Mater. Process. Technol. 2016;228:11–24. https://doi.org/10.1016/j.jmatprotec.2015.09.023.
[37] Salvado FC, Teixeira-Dias F, Walley SM, Lea LJ, Cardoso JB. A review on the strain rate dependency of the dynamic viscoplastic response of FCC metals. Prog. Mater. Sci. 2017;88:186–231. https://doi.org/10.1016/j.pmatsci.2017.04.004.
[38] Wu Y, Liu G, Wang K, Liu Z, Yuan S. The deformation and microstructure of Ti-3Al-2.5V tubular component for non-uniform temperature hot gas forming. Int. J. Adv. Manuf. Technol. 2016;88:2143–52. https://doi.org/10.1007/s00170-016-8927-3.
[39] Havner KS. On the onset of necking in the tensile test. Int. J. Plast. 2004;20:965–78. https://doi.org/10.1016/j.ijplas.2003.05.004.

[40] Zheng P, Chen R, Liu H, Chen J, Zhang Z, Liu X, et al. On the standards and practices for miniaturized tensile test – a review. Fusion Eng. Des. 2020;161. https://doi.org/10.1016/j.fusengdes.2020.112006.
[41] Tu S, Ren X, He J, Zhang Z. Stress–strain curves of metallic materials and post-necking strain hardening characterization: a review. Fatigue Fract. Eng. Mater. Struct. 2019;43:3–19. https://doi.org/10.1111/ffe.13134.
[42] Zheng Q, Furushima T. Evaluation of high-temperature tensile behavior for metal foils by a novel resistance heating assisted tensile testing system using samples with optimized structures. J. Mater. Sci. Technol. 2021;94:216–29. https://doi.org/10.1016/j.jmst.2021.03.061.